

RESEARCH

Spike Train Cumulants for Linear-Nonlinear Poisson Cascade Models

Michael Kordovan and Stefan Rotter

Full list of author information is
available at the end of the article

Abstract

Spiking activity in cortical networks is nonlinear in nature. The linear-nonlinear cascade model, some versions of which are also known as point-process generalized linear model, can efficiently capture the nonlinear dynamics exhibited by such networks. Of particular interest in such models are theoretical predictions of spike train statistics. However, due to the moment-closure problem, approximations are inevitable. We suggest here a series expansion that explains how higher-order moments couple to lower-order ones. Our approach makes predictions in terms of certain integrals, the so-called loop integrals. In previous studies these integrals have been evaluated numerically, but numerical instabilities are sometimes encountered rendering the results unreliable. Analytic solutions are presented here to overcome this problem, and to arrive at more robust evaluations. We were able to deduce these analytic solutions by switching to Fourier space and making use of complex analysis, specifically Cauchy's residue theorem. We formalized the loop integrals and explicitly solved them for specific response functions. To quantify the importance of these corrections for spike train cumulants, we numerically simulated spiking networks and compared their sample statistics to our theoretical predictions. Our results demonstrate that the magnitude of the nonlinear corrections depends on the working point of the nonlinear network dynamics, and that it is related to the eigenvalues of the mean-field stability matrix. For our example, the corrections for the firing rates are in the range between 4 % and 21 % on average. Precise and robust predictions of spike train statistics accounting for nonlinear effects are, for example, highly relevant for theories involving spike-timing dependent plasticity (STDP).

Keywords: Spike train cumulants; Linear-nonlinear Poisson model; Path integral formalism; Structure-dynamics relations

1 Introduction

Novel experimental techniques for neuronal recordings generate huge volumes of data. These data contain information about neuronal spike trains, the firing rate of individual neurons, and correlations between neurons, but also information about their connectivity [1–10].

Modeling neuronal activity can be performed at different scales [11]. The largest amount of neurophysiological detail is conveyed by the simulation of neuron models with dendrites and axons extending in three-dimensional space [12]. Apart from the problem that most of the details concerning neuron morphology and ion channel equipment are not known, this approach is computationally very demanding, and may become entirely unfeasible for larger networks of neurons. Consequently, most studies of large-scale spiking network dynamics use simpler point neuron models. They come as deterministic or stochastic units. A well-known example of the former type is the *leaky integrate-and-fire neuron* [13, 14], a prominent representative of the latter are self-exciting and mutually-exciting Poisson processes, called *Hawkes processes* [15, 16]. Studying biophysically inspired models and abstract point processes side-by-side can be of great help to understand the influence of network structure on spike train statistics in recurrent networks [17–20].

As the classical Hawkes model is fully linear, the nonlinear dynamics of biological neuronal networks must be linearized before comparing them. This poses limits to the range of applications of this model, and to the precision of the results achieved with it. A natural generalization emerges by including an arbitrary transfer function for the firing rates to account for intrinsic neuronal nonlinearities. Such a model, called *linear-nonlinear Poisson (LNP) cascade model*, naturally emerges for several spiking neuron models [21]. As a phenomenological model, it has also been successfully employed for the analysis of multiple-neuron spike trains [22–25].

Computing spike train cumulants of any order in the LNP model is a daunting task. However, the precise knowledge of certain low-order cumulants is of great importance for the study of spike-timing dependent plasticity (STDP) [26]. For simple pairwise STDP, first- and second-order cumulants are sufficient, but the more complex model of triplet STDP [27] requires accurate knowledge of third-order spike train cumulants. Furthermore, there is evidence that higher-order cumulants constrain neuronal activity patterns, and it has been shown that including them into

statistical models improves the fit of experimental data [28]. For predictions in non-linear models, the coupling of higher-order moments to lower-order ones complicates the calculations. This issue is known as the *moment-closure problem*. One systematic way to deal with this problem and to manage the complexity of the hierarchy of contributions has been proposed by [29] in terms of a path integral formulation. The authors in [30] used this method to calculate perturbative corrections to the predictions made by the linear model. The corrections arise as higher-order moments couple to lower-order ones, due to the nonlinearity.

In principle, the problem might be considered to be solved, and in theory it is. But when it comes to actual numerical predictions of cumulants, several technical difficulties arise. In the diagrammatic expansion, corrections stemming from the nonlinear transfer functions involve diagrams with loops. When calculating the contributions of these loop diagrams, integrals over the loop momentum have to be solved. Only analytic solutions guarantee a correct solution of these integrals, independent of choices made for the parameters. Here we demonstrate how loop integrals can be analytically solved using methods from complex analysis. For certain parameter regimes numerical estimates can be misleading (or wrong) and analytic solutions are preferred.

2 Spiking Model and Methods

In a network of spiking units, the individual node activities generally depend on different variables. These variables reflect the applied stimulus, previous history of activity, and neuronal coupling [31]. We first review a widely used stochastic model, and then outline a less well-known representation of it [30].

2.1 Linear-nonlinear Poisson cascade model

Dynamics in neuronal networks can be mathematically described as stochastic point processes [32]. The spikes associated to a neuron in a network correspond to discrete events in time. Individual spikes are random but not necessarily stochastically independent [23, 25, 32].

A point process can be defined by use of discrete event times, inter-event intervals, or a cumulative counting process [33, 34]. A *point process* is a random sequence $\mathcal{T} = [t^\gamma]_{\gamma \geq 1}$ with $t^0 = 0$, $t^\gamma \in [0, \infty)$ and $t^\gamma < t^{\gamma+1}$ [34]. A useful representation of

a point process is given by the collection of all events,

$$z(t) = \sum_{t^\gamma} \delta(t - t^\gamma), \quad (1)$$

where $\delta(t)$ is the Dirac measure. The associated counting process $N(t)$ is given by

$$N(t) = \int_0^t z(t) dt. \quad (2)$$

If $\mathcal{P}[N(t, t+x) = k]$ only depends on the duration x , but not on the location t , the point process is called *crudely stationary* [34]. For crudely stationary point processes, Khinchin's Existence Theorem [34, Proposition 3.3.I] guarantees the existence of the intensity

$$\lambda = \lim_{dt \searrow 0} \frac{\mathcal{P}[N(0, t] > 0]}{dt}, \quad (3)$$

although it might be infinite. In case of finite intensities, it is meaningful to write

$$\mathcal{P}[N(t, t+dt) > 0] = \lambda dt + o(dt). \quad (4)$$

Further, a point process is said to be *simple* [34], if

$$\mathcal{P}[N(\{t\}) = 0 \text{ or } 1 \ \forall t] = 1. \quad (5)$$

A crudely stationary point process is *orderly* [34], when

$$\mathcal{P}[N(0, dt) \geq 2] = o(dt), \quad (dt \searrow 0). \quad (6)$$

For crudely stationary point processes of finite intensity, these two properties are equivalent [34]. The most prominent example is a stationary Poisson process, completely defined by [34]

$$\mathcal{P}[N(a_i, b_i) = n_i, i = 1, \dots, k] = \prod_{i=1}^k \frac{(\lambda(b_i - a_i))^{n_i}}{n_i!} e^{-\lambda(b_i - a_i)}, \quad (7)$$

with $a_i < b_i \leq a_{i+1}$.

In a multivariate setting, each neuron i has an associated point process \mathcal{T}_i describing its spike times. The corresponding point process representation $z_i(t)$ from

Eq. (1) is called *spike train*. The *spike count* of neuron i is the counting process $N_i(t)$ associated with \mathcal{T}_i . It is defined by

$$N_i(t) = \sum_{\gamma=1}^{\infty} \Theta(t - t_i^\gamma), \quad (8)$$

or equivalently

$$N_i(t) = \int_0^t z_i(t) dt. \quad (9)$$

Assuming orderliness, a multivariate counting Process $(N_i(t), \dots, N_n(t))_{t \geq 0}$ is entirely characterized by its conditional intensity process $(\lambda_i(t), \dots, \lambda_n(t))_{t \geq 0}$. For finite intensity processes we may write

$$\mathcal{P}[dN_i(t) = 1 | \mathcal{H}_t] = \lambda_i(t) dt, \quad (10)$$

where \mathcal{H}_t is the history of the point process up to time t [33].

An interesting candidate is given by linear-nonlinear cascade models [21, 35, 36], where the intensities read

$$\lambda_i(t) = \phi_i \left(\sum_j \int_{-\infty}^{t-} h_{ij}(t-s) dN_j(s) + b_i(t) \right). \quad (11)$$

Here, h_{ij} is the (causal) response function describing the influence that neuron j exerts on neuron i . The nonnegative gain function ϕ_i accounts for the nonlinear transfer from the intrinsic state (“membrane potential”) to the intensity (“firing rate”), and $b_i(t)$ specifies the baseline intensity. The linear filtering can be thought of as the spatiotemporal receptive field of the neuron under investigation [35]. By use of Eq. (9), we have

$$\lambda_i(t) = \phi_i \left(\sum_j (h_{ij} \star z_j)(t) + b_i(t) \right), \quad (12)$$

where $(f \star g)(t)$ denotes the usual convolution operation. Integration boundaries and causality are reflected by an appropriate definition of h_{ij} .

The connectivity in a neuronal network is specified by the adjacency matrix A with entries $a_{ij} \in \{0, 1\}$, or $a_{ij} \in \mathbb{N}_0$ if multiple connections are allowed between two neurons. As the effects on post-synaptic neurons can vastly differ in magnitude,

and synapses can be either excitatory or inhibitory, synapses carry a signed weight w_{ij} . The connectivity matrix W is given by a Hadamard product of adjacency matrix and weight matrix. Finally, any time-dependencies of the neuronal influence are reflected by the synaptic kernel functions. They might vary for different neuron types and thus, the matrix of causal interaction filters $H = (h_{ij})_{i,j \in \{1, \dots, n\}}$ is the Hadamard product of the matrix of response functions and the connectivity matrix.

We term this model *linear-nonlinear Poisson (LNP) cascade model* similar to [36]. Poisson means that spikes are drawn from a Poisson distribution with instantaneous rate λ , but due to the self-interaction and history dependence the output spike trains do clearly not fulfill the independence criteria of an inhomogeneous Poisson process any more. These processes are further known as (nonlinear) Hawkes processes if all interactions are non-negative [34, 37, 38].

A different formulation which is better suited for estimation of these processes is obtained by means of the point process generalized linear model framework [23, 39]. More specifically, the joint probability density of the process is approximated by a discrete one. This defines a likelihood function belonging to the exponential family with canonical parameter $\log \lambda_i(t)$ [22, 39]. In the generalized linear model setting this canonical parameter is expressed as linear combination of covariates [40]. Thus, the LNP cascade model with exponential gain function can directly be obtained [22, 24]. The exponential gain function further implies multiplicative effects from previous spikes on the instantaneous firing rates [41]. Point process generalized linear models are very promising and successful models for spike responses of single neurons or networks [23, 31, 35, 39, 42].

A concluding remark concerns the nonlinear gain function. Nonlinearities can enter at two different levels, pre-synaptic or post-synaptic, corresponding to the connectivity matrix appearing outside or inside the nonlinearity. For the former, an Amari-type model [43, 44], the rate is given by

$$\lambda_i(t) = \kappa \sum_j W_{ij} \phi(z_j(t)) + b_i(t). \quad (13)$$

Both models imply different corrections to mean-field equations as pointed out by [45]. A further possibility to incorporate nonlinearities into the model is by

considering Volterra series expansions. Recent progress in this direction can be found in [46].

2.2 Path integral representation of the linear-nonlinear Poisson cascade model

Since the moment generating functional for the LNP cascade model cannot be calculated analytically, the following alternative strategy is applied. First, an auxiliary variable, the so-called *response variable*, is introduced. Its dynamics describes the stochastic evolution of the system under consideration [30]. Then, the probability density functional (pdf) of the process is written in exponential form, where the negative exponent is called the *action*. The action splits into the *free action*, which is bilinear in the configuration and the response variable, and the *interaction* component, which comprises all remaining terms. While expectation values with respect to the pdf of the free action can be calculated, this is generally not possible for the full action. However, the interaction component can be expanded into a series. Finally, the moments of the process are calculated in a perturbative manner as sums of free moments.

A derivation of the path integral representation can be found in [30]. In case of the response function h being chosen as α -function, [47] derived an explicit path integral representation for the shot noise variable $s(t) = \sum_{t^\gamma} h(t - t^\gamma)$.

In brief, the line of reasoning in deriving the action of the LNP cascade model follows arguments from nonequilibrium statistical dynamics [48–53]. For illustration, we consider the case $n = 1$ and drop the neuron index i . Starting at time t^0 and discretizing time into N_t steps of size Δt

$$t^{\nu+1} = t^\nu + \Delta t, \quad \nu = 0, 1, \dots, N_t - 1, \quad (14)$$

we obtain a discrete spike count $N^\nu = N(t^\nu)$ and a discretized intensity process $\lambda^\nu = \lambda(t^\nu)$. In the following, we set $N^0 = 0$. Given conditionally independent Poissonian increments, the spike counting process reads

$$N^{\nu+1} = N^\nu + \eta^\nu, \quad \eta^\nu \sim \text{Poiss}(\Delta t \lambda^\nu). \quad (15)$$

Starting point in deriving the action is the pdf written in terms of δ -functions constrained to the solutions of Eq. (15),

$$\begin{aligned} P[(N^1, \dots, N^{N_t}) | (\eta^0, \dots, \eta^{N_t-1}), N^0 = 0] &= \prod_{\nu=0}^{N_t-1} \delta(N^{\nu+1} - N^\nu - \eta^\nu) \\ &= \int \left(\prod_{\nu=0}^{N_t-1} \frac{d\tilde{z}^\nu}{2\pi i} \right) \exp \left(- \sum_{\nu} \tilde{z}^\nu (N^{\nu+1} - N^\nu - \eta^\nu) \right). \end{aligned} \quad (16)$$

In the second step, the Laplace representation

$$\delta(x) = \frac{1}{2\pi i} \int e^{\tilde{z}x} d\tilde{z} \quad (17)$$

of the δ -function has been used for all ν . Note that the integration over \tilde{z} is along the imaginary axis.

In general, the Poisson probability density function for variables k and mean parameter λ is given by

$$P_\lambda(k) = \frac{\lambda^k}{k!} e^{-\lambda}. \quad (18)$$

The moment generating function for such a process reads

$$\begin{aligned} Z[J] &= \langle e^{Jk} \rangle = \sum_{k=0}^{\infty} \frac{\lambda^k}{k!} e^{-\lambda} e^{Jk} = e^{-\lambda} e^{\lambda e^J} \\ &= \exp(\lambda(e^J - 1)). \end{aligned} \quad (19)$$

Noise increments η^ν are conditionally independent, which implies

$$P[\eta^0, \dots, \eta^{N_t-1}] = \prod_{\nu} P(\eta^\nu | \lambda^\nu). \quad (20)$$

Marginalizing the pdf (16) over the noise increments yields

$$\begin{aligned} P[(N^1, \dots, N^{N_t}) | N^0 = 0] &= \sum_{\eta^0} \dots \sum_{\eta^{N_t-1}} \\ &P[(N^1, \dots, N^{N_t}) | (\eta^0, \dots, \eta^{N_t-1}), N^0 = 0] \prod_{\nu=0}^{N_t-1} P_{\Delta t \lambda^\nu}(\eta^\nu). \end{aligned} \quad (21)$$

Note that for one particular noise increment one has

$$\begin{aligned} \sum_{\eta^\nu} e^{-\tilde{z}^\nu(-\eta^\nu)} \cdot \frac{(\Delta t \lambda^\nu)^{\eta^\nu}}{\eta^\nu!} e^{-\Delta t \lambda^\nu} &= \langle e^{\tilde{z}^\nu \eta^\nu} \rangle \\ &= Z[\tilde{z}^\nu] = \exp \left(\Delta t \lambda^\nu (e^{\tilde{z}^\nu} - 1) \right). \end{aligned} \quad (22)$$

Substituting this result into the marginalized pdf (21) yields

$$\begin{aligned} P[(N^1, \dots, N^{N_t}) | N^0 = 0] &= \int \left(\prod_{\nu=0}^{N_t-1} \frac{d\tilde{z}^\nu}{2\pi i} \right) \exp \left(- \sum_{\nu} \tilde{z}^\nu (N^{\nu+1} - N^\nu) \right) \\ &\quad \times \exp \left(\sum_{\nu} \Delta t \lambda^\nu (e^{\tilde{z}^\nu} - 1) \right). \end{aligned} \quad (23)$$

As a next step, the limit of infinitesimal step size Δt and infinitely many steps ($N_t \rightarrow \infty$) is performed, while keeping the total time $T = N_t \Delta t$ constant. This turns sums into integrals

$$\lim_{\Delta t \rightarrow 0} \sum_{\nu=0}^{N_t=T/\Delta t} \Delta t \cdot f(\nu \Delta t) = \int_0^T f(t) dt. \quad (24)$$

The full path integral then reads

$$\begin{aligned} P[z|z(0) = 0] &= \int \mathcal{D}\tilde{z} \exp \left\{ - \int_{t^0}^T \tilde{z}(t) z(t) dt \right. \\ &\quad \left. + \int_{t^0}^T \lambda(t) (e^{\tilde{z}(t)} - 1) dt \right\}, \end{aligned} \quad (25)$$

with $\mathcal{D}\tilde{z} = \lim_{N_t \rightarrow \infty} \prod_{\nu=0}^{N_t-1} \frac{d\tilde{z}^\nu}{2\pi i}$ and $\lim_{\Delta t \rightarrow 0} \frac{N(t+\Delta t) - N(t)}{\Delta t} = z(t)$. Conventionally one writes the pdf $P[z|z(0) = 0]$ as a path integral over the so-called path density $\mathfrak{p}[\tilde{z}, z]$ which is itself an exponential of the negative action $-S[\tilde{z}, z]$

$$\begin{aligned} P[z|z(0) = 0] &= \int \mathcal{D}\tilde{z} \exp(-S[\tilde{z}, z]) \\ &= \int \mathcal{D}\tilde{z} \mathfrak{p}[\tilde{z}, z]. \end{aligned} \quad (26)$$

Thus, the action for a LNP cascade process for $n = 1$ reads

$$S[\tilde{z}, z] = \int \tilde{z}(t) z(t) - (e^{\tilde{z}(t)} - 1) \phi((h \star z)(t) + b(t)) dt. \quad (27)$$

As everything factorizes, the action of the LNP model for more than one neuron ($n > 1$) is finally given by [30],

$$S_{\text{LNP}}[\tilde{z}, z] = \sum_i \int \tilde{z}_i(t) z_i(t) - \left(e^{\tilde{z}_i(t)} - 1 \right) \phi \left(\sum_j (h_{ij} \star z_j)(t) + b_i(t) \right) dt. \quad (28)$$

Proceeding with the action $S_{\text{LNP}}[\tilde{z}, z]$ directly would yield an expansion about $z = 0$. However, a different expansion point can be chosen by shifting the configuration and response variables by \bar{r} and \tilde{r} , respectively. Transforming the variables according to

$$z_i \longrightarrow \delta z_i = z_i - \bar{r}_i, \quad (29)$$

$$\tilde{z}_i \longrightarrow \delta \tilde{z}_i = \tilde{z}_i - \tilde{r}_i, \quad (30)$$

results in an action $S^*[\delta \tilde{z}, \delta z]$. Shifting the processes by its first moments, $\bar{r}_i = \langle z_i \rangle$ and $\tilde{r}_i = \langle \tilde{z}_i \rangle$, yields an *effective action* [54]. As the action is at least linear in the auxiliary response variable, its first moment $\langle \tilde{z}_i \rangle$ is zero and the transformation of \tilde{z}_i is trivial.

The general Taylor expansion of ϕ about \bar{r} is given by

$$\phi \left(\sum_j (h_{ij} \star z_j)(t) + b_i(t) \right) = \phi \left(\sum_j (h_{ij} \star \delta z_j)(t) + \sum_j (h_{ij} \star \bar{r}_j)(t) + b_i(t) \right) \quad (31)$$

$$= \sum_{q=0}^{\infty} \frac{1}{q!} \phi_i^{(q)} (h \star \delta z)_i^q(t), \quad (32)$$

where $(h \star \delta z)_i(t) = \sum_j (h_{ij} \star \delta z_j)(t)$ and coefficients

$$\phi_i^{(q)} = \frac{d^q}{dx^q} \phi(x)|_{(h \star \bar{r})_i + b_i}. \quad (33)$$

Raising the convolution to the power of q is meant to be

$$(h \star \delta z)_i^q(t) = \underbrace{(h \star \delta z)_i(t) \times \cdots \times (h \star \delta z)_i(t)}_{q \text{ times}}. \quad (34)$$

The action with transformed variables then reads

$$S^*[\tilde{z}, \delta z] = \sum_i \int dt \left[\tilde{z}_i(t) \delta z_i(t) + \tilde{z}_i(t) \bar{r}_i(t) - \underbrace{\left(e^{\tilde{z}_i(t)} - 1 \right)}_{=\sum_{p=1}^{\infty} \frac{(\tilde{z}_i(t))^p}{p!}} \left(\sum_{q=0}^{\infty} \frac{1}{q!} (h \star \delta z)_i^q(t) \right) \right]. \quad (35)$$

For moment calculations, the bilinear part of the action is split off

$$S^*[\tilde{z}, \delta z] = S_F[\tilde{z}, \delta z] + S_I^*[\tilde{z}, \delta z], \quad (36)$$

where the free (bilinear) action reads

$$S_F[\tilde{z}, \delta z] = \sum_i \int dt \tilde{z}_i(t) \left(\delta z_i(t) - \phi_i^{(1)}(h \star \delta z)_i \right). \quad (37)$$

The component representing the interaction is given by

$$S_I^*[\tilde{z}, \delta z] = - \sum_i \int dt \sum_{\substack{p=1, q=0 \\ \setminus \{p=q=1\} \\ \setminus \{p=1, q=0\}}} \frac{(\tilde{z}_i(t))^p}{p!} \frac{\phi_i^{(q)}}{q!} (h \star \delta z)_i^q(t) + \sum_i \int dt \tilde{z}_i(t) \left(\bar{r}_i(t) - \phi_i^{(0)} \right). \quad (38)$$

The *inverse tree-level propagator* is defined by the bilinear part S_F of the action,

$$\Delta_{T,ij}^{-1}(t, t') = \delta_{ij} \delta(t - t') - \phi_i^{(1)} h_{ij}(t - t'). \quad (39)$$

Finally, the tree-level propagator can be deduced from

$$\sum_k \int dt' \Delta_{T,ik}^{-1}(t, t') \Delta_{T,kj}(t', t'') = \delta(t - t'') \delta_{ij}. \quad (40)$$

In this representation, *tree* and *loop* level refer to zeroth order and first order, respectively, in a small-fluctuation expansion in terms of higher-order moments coupling to lower-order ones [54, 55]. This expansion is called semiclassical expansion, or loop expansion, because the number of loops in a diagram corresponds to higher-order fluctuation contributions [30, 55]. Whenever fluctuations are small, the truncated loop expansion provides a good approximation for spike train statistics.

In the following, the expansion is performed about the mean-field solution, instead of choosing $\bar{r} = 0$. Very recently, [56] used renormalization group techniques to self-

consistently determine the statistics of the process. An application of these methods to our model still needs to be investigated. Here, we consider an approximation, where the expansion point is determined by the free (tree-level) expectation

$$\bar{r}_i(t) = \langle z_i(t) \rangle_F = \phi_i^{(0)}, \quad (41)$$

where $\langle \cdot \rangle_F$ denotes the expectation with respect to the free path density $\exp(-S_F)$. The true mean of the process is different for nonlinear gain functions, as there are non-vanishing loop corrections to the mean (cf. Section 3.3.1).

By Eq. (41), the last term in Eq. (38) vanishes and the interacting action reads

$$S_I^{\text{MF}}[\tilde{z}, \delta z] = - \sum_i \int dt \sum_{\substack{p=1, q=0 \\ \setminus \{p=q=1\} \\ \setminus \{p=1, q=0\}}} \frac{(\tilde{z}_i(t))^p}{p!} \frac{\phi_i^{(q)}}{q!} (h \star \delta z)_i^q(t). \quad (42)$$

In total, the action of the LNP model expanded about its mean-field solution reads

$$S^{\text{MF}}[\tilde{z}, \delta z] = S_F[\tilde{z}, \delta z] + S_I^{\text{MF}}[\tilde{z}, \delta z]. \quad (43)$$

The path-integral representation of the probability density functional is given by

$$P[\delta z | \delta z(0)] = \int \mathcal{D}\tilde{z}(t) \exp(-S^{\text{MF}}[\tilde{z}, \delta z]), \quad (44)$$

where $\mathcal{D}\tilde{z}$ denotes the path integral measure. This implies a joint moment-generating functional of δz and \tilde{z}

$$Z[J, \tilde{J}] = \int \mathcal{D}z(t) \int \mathcal{D}\tilde{z}(t) e^{-S^{\text{MF}}[\tilde{z}, \delta z] + J\tilde{z} + \tilde{J}\delta z}, \quad (45)$$

and a moment-generating functional of δz

$$Z[\tilde{J}] = \int \mathcal{D}z(t) e^{-S^{\text{MF}}[\tilde{z}, \delta z] + \tilde{J}\delta z}. \quad (46)$$

As a consequence of the splitting in Eq. (43), arbitrary moments of the process can be calculated as a combination of moments of the free action

$$\begin{aligned} \left\langle \prod_{\iota=1}^l \delta z_{i_\iota}(t_\iota) \prod_{\varsigma=1}^m \tilde{z}_{i_\varsigma}(t_\varsigma) \right\rangle &= \int \mathcal{D}\delta z \mathcal{D}\tilde{z} \prod_{\iota=1}^l \delta z_{i_\iota}(t_\iota) \prod_{\varsigma=1}^m \tilde{z}_{i_\varsigma}(t_\varsigma) e^{-S^{\text{MF}}[\tilde{z}, \delta z]} \\ &= \left\langle \prod_{\iota=1}^l \delta z_{i_\iota}(t_\iota) \prod_{\varsigma=1}^m \tilde{z}_{i_\varsigma}(t_\varsigma) \prod_{\substack{p,q=1 \\ \setminus \{p=q=1\} \\ \setminus \{p=1,q=0\}}} \sum_{k=0}^{\infty} \frac{1}{k!} \left(\frac{\tilde{z}_i^p}{p!} \frac{\phi_i^{(q)}}{q!} (h \star \delta z)_i^q \right)^k \right\rangle_F, \end{aligned} \quad (47)$$

where $\langle \cdot \rangle_F$ again denotes the expectation with respect to the free path density $\exp(-S_F)$. By completing the square and using the definition of the inverse tree-level propagator, the moment-generating functional of the free moments reads

$$Z_F[\tilde{J}, J] = \exp \left\{ \int dt \int dt' \tilde{J}(t) \Delta_T(t, t') J(t') \right\}. \quad (48)$$

This functional is bilinear and thus only products of tree-level propagators survive when calculating free moments

$$\left\langle \prod_{\iota=1}^l \delta z_{i_\iota}(t_\iota) \prod_{\varsigma=1}^m \tilde{z}_{i_\varsigma}(t_\varsigma) \right\rangle_F = \sum_{\text{pair-wise partitions}} \prod_{\text{pairs } (\iota, \varsigma)} \Delta_{T, i_\iota i_\varsigma}(t_\iota, t_\varsigma). \quad (49)$$

The expansion of Eq. (47) can be represented diagrammatically by use of the observation (49). Contributions from individual components of the series are obtained by the Feynman rules listed in the following section and derived in [30].

2.2.1 Feynman rules of the LNP cascade model

The Feynman rules in this section are derived for computing cumulant expansions about the mean-field solution $\bar{r} = \langle z \rangle_F$, considering S^{MF} from Eq. (43). For book-keeping reasons, each term in Eq. (47) is represented by a Feynman diagram. The building blocks of these diagrams are

- external vertices according to the desired moment

$$\bigcirc \longleftarrow \dots = 1$$

$$\dots \longrightarrow \bigcirc = 1$$

- the propagator

$$\begin{array}{c} t_1 \quad \quad t_2 \\ \xleftarrow{\quad} \\ i \quad \quad j \end{array} = \Delta_{T,ij}(t_1, t_2)$$

- the filter edge

$$\begin{array}{c} t_2 \quad \quad t_1 \\ \text{~~~~~} \\ i \quad \quad j \end{array} = h_{ij}(t_2 - t_1)$$

- the filter vertex

$$\begin{array}{c} t \\ \text{~~~~~} \bullet \xleftarrow{\quad} \\ i \quad \quad j \end{array} = \delta_{ij}$$

- the internal vertices

$$\begin{array}{c} i_1 \quad \quad j_1 \\ \diagdown \quad \diagup \\ \vdots \quad \quad \vdots \\ p \text{ legs} \quad \bullet \quad q \text{ legs} \\ \diagup \quad \diagdown \\ i_p \quad \quad j_q \end{array} = \frac{\phi_{i_1}^{(q)}}{p!q!} \prod_{\iota=2}^p \delta_{i_1 i_\iota} \prod_{\varsigma=1}^q \delta_{i_1 j_\varsigma},$$

where $\phi_i^{(q)}$ has been defined in Eq. (33). From Eq. (47) it is obvious that $p \geq 2$ for $q = 0$. Otherwise, any combination is allowed such that $q + p \geq 3$.

The moment expansion given in Eq. (47) allows to deduce an algorithmic recipe to calculate cumulants. Note that these are calculated about the mean-field solution \bar{r} , i.e. $\langle \delta z \rangle_T = 0$. The n^{th} order cumulant is obtained by the following recipe

- 1 Determine all possible graphs, where the cumulant order corresponds to the external vertices and the perturbation order corresponds to inner vertices.
- 2 Translate vertices and edges into formulae according to the building blocks described above.
- 3 Integrate over internal vertex times $\int dt_\xi$ and sum over neuron indices.
- 4 If a vertex type occurs k times (from $(S_I[\tilde{z}, \delta z])^k$ terms) include a factor $1/k!$.
- 5 For n_{sym} topologically identical graphs, multiply with the factor n_{sym} (corresponding to possible pairings in Eq. (49)).

A frequently recurring sub-diagram is the combination of a filter edge, a filter vertex, and the propagator. We therefore introduce the shorthand

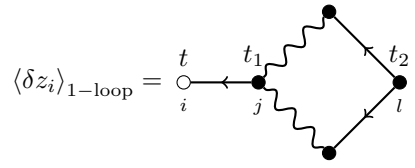
$$(h \star_1 \Delta_T)_{ij}(t, t'') = \sum_k \int dt' h_{ik}(t - t') \Delta_{T,kj}(t', t''). \quad (50)$$

We will use these rules to deduce explicit predictions in the following section.

3 Results

3.1 Techniques for calculating loop corrections

A procedure to compute higher-order cumulants and their corrections arising from the nonlinear transfer function was described in the previous section. However, there are some technical obstacles to actually calculate them. For an example, consider the one-loop correction to the firing rates



$$\begin{aligned} \langle \delta z_i \rangle_{1\text{-loop}} &= 2 \cdot \sum_{j,l} \int \Delta_{T,ij}(t, t_1) \frac{\phi_j^{(2)}}{1!2!} (h \star_1 \Delta_T)_{jl}(t_1, t_2) (h \star_1 \Delta_T)_{jl}(t_1, t_2) \\ &\quad \times \frac{\phi_l^{(0)}}{2!} dt_1 dt_2. \end{aligned}$$

The depicted Feynman diagram is the only one possible with one loop for the first-order cumulant. It is translated into a formula in accordance with the Feynman rules described in Section 2.2.1. For a stationary process, the one-loop correction of the mean is time-independent. Computations are simpler in the Fourier domain, as temporal integration is eliminated

$$\begin{aligned} \langle \delta z_i \rangle_{1\text{-loop}} &= \frac{1}{4\pi} \sum_{j, k_1, k_2, l} \int \hat{\Delta}_{T,ij}(0) \phi_j^{(2)} \hat{h}_{jk_1}(-\omega) \hat{\Delta}_{T,k_1l}(-\omega) \\ &\quad \times \hat{h}_{jk_2}(\omega) \hat{\Delta}_{T,k_2l}(\omega) \phi_l^{(0)} d\omega. \end{aligned} \quad (51)$$

Further details on this calculation can be found later in Section 3.3.1. Here we just note that one is left with the frequency integration

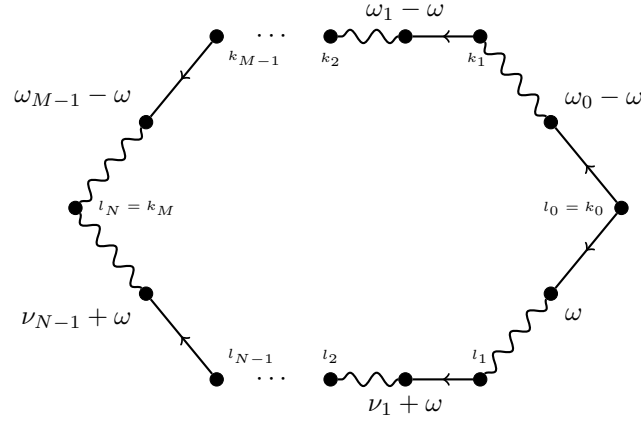
$$\sum_{k_1, k_2} \int_{-\infty}^{\infty} \hat{h}_{jk_1}(-\omega) \hat{\Delta}_{T,k_1l}(-\omega) \hat{h}_{jk_2}(\omega) \hat{\Delta}_{T,k_2l}(\omega) d\omega. \quad (52)$$

The authors in [30] solved these integrals numerically by performing Riemann summation for a fixed range of frequencies. Due to the analytic nature of the integrands, however, this approach is error-prone and may even fail completely.

In the following, a technique is presented which allows to calculate these integrals analytically for common choices of the response functions. After formalizing the loop integrals, all results will be assembled. As a consequence, the following section is rather technical. We are using the explicit computations of first-order and second-order cumulants in Section 3.3 and compare them to a numerical simulation in Section 3.4.

3.2 General loop integrals

A frequently occurring one-loop integral is characterized by the number of propagators in the loop



Note that legs entering or leaving the loop have been omitted at this point, and an ambiguity in the indices ($l_0 = k_0$ and $l_N = k_M$) is introduced for ease of notation. Later, this issue will be resolved by appropriate Kronecker δ 's. To calculate corrections involving these loops as part of the diagram, we define a general loop integral in Fourier space

$$\begin{aligned} \mathcal{L}_{k_M \dots k_0, l_N \dots l_0}(\vec{\omega}, \vec{\nu}) &= \int E_{k_M k_{M-1}}(\omega_{M-1} - \omega) \cdots E_{k_2 k_1}(\omega_1 - \omega) \\ &\times E_{k_1 k_0}(\omega_0 - \omega) E_{l_N l_{N-1}}(\nu_{N-1} + \omega) \cdots E_{l_2 l_1}(\nu_1 + \omega) E_{l_1 l_0}(\omega) d\omega \end{aligned} \quad (53)$$

where $\vec{\omega} = (\omega_0, \dots, \omega_{M-1})$ and $\vec{\nu} = (\nu_1, \dots, \nu_{N-1})$. A loop edge E in Fourier space is the combination of a filter edge and a propagator (cf. Eq. (50)) and is given by

$$E_{ij}(\omega) = \sum_k \hat{h}_{ik}(\omega) \hat{\Delta}_{T,kj}(\omega). \quad (54)$$

For an analytic solution, we aim to calculate the integrals \mathcal{L} . First, note that the ω -dependence of the Fourier transformed propagator $\hat{\Delta}_T(\omega)$ is completely determined by the Fourier transform $\hat{h}(\omega)$ of the response function, which is assumed to

be the same for all neurons. We define $D_{\phi^{(1)}} = \text{diag}\{\phi_1^{(1)}, \dots, \phi_n^{(1)}\}$ and exploit a diagonalization of the matrix $D_{\phi^{(1)}}W$

$$V^{-1}D_{\phi^{(1)}}WV = \text{diag}\{\xi_1, \dots, \xi_n\}, \quad (55)$$

where ξ_i denotes the i -th eigenvalue of $D_{\phi^{(1)}}W$. Assuming that the matrix $D_{\phi^{(1)}}W$ is diagonalizable considerably simplifies all subsequent calculations. If this is not the case, one would consider the Jordan canonical form and extend the following computations in a suitable way. For the Fourier transformed tree-level propagator determined from Eq. (40), it follows that

$$\begin{aligned} \widehat{\Delta}_T(\omega) &= \left(\mathbb{1} - D_{\phi^{(1)}}\widehat{h}(\omega)W \right)^{-1} \\ &= V \text{diag}\left\{ \frac{1}{1 - \widehat{h}(\omega)\xi_1}, \dots, \frac{1}{1 - \widehat{h}(\omega)\xi_n} \right\} V^{-1}. \end{aligned} \quad (56)$$

Defining

$$D_i(\omega) = \frac{\widehat{h}(\omega)}{1 - \widehat{h}(\omega)\xi_i} \quad (57)$$

and assuming the same response function h for all neurons, the loop edge E reads

$$E_{ij}(\omega) = \sum_k (WV)_{ik} D_k(\omega) V_{kj}^{-1}. \quad (58)$$

The integrals to be solved are

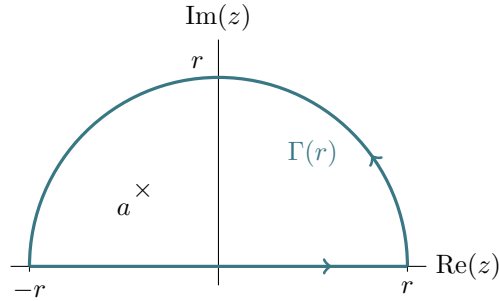
$$\mathcal{I}_{i_0 \dots i_{M-1}, j_0 \dots j_{N-1}}(\vec{\omega}, \vec{\nu}) = \int \prod_{\iota=0}^{M-1} D_{i_\iota}(\omega_\iota - \omega) D_{j_0}(\omega) \prod_{\varsigma=1}^{N-1} D_{j_\varsigma}(\nu_\varsigma + \omega) d\omega. \quad (59)$$

In what follows, we are sometimes only considering the integrand of these integrals $\mathcal{I}_{i_0 \dots i_{M-1}, j_0 \dots j_{N-1}}$ which is then denoted by $I_{i_0 \dots i_{M-1}, j_0 \dots j_{N-1}}$. Given these integrals, the loop integral reads

$$\begin{aligned} \mathcal{L}_{k_M \dots k_0, l_N \dots l_0}(\vec{\omega}, \vec{\nu}) &= \sum_{i_0, \dots, i_{M-1}} \sum_{j_0, \dots, j_{N-1}} \mathcal{I}_{i_0 \dots i_{M-1}, j_0 \dots j_{N-1}}(\vec{\omega}, \vec{\nu}) \\ &\quad \times \prod_{\iota=0}^{M-1} (WV)_{k_{\iota+1} i_\iota} V_{i_\iota k_\iota}^{-1} \prod_{\varsigma=0}^{N-1} (WV)_{l_{\varsigma+1} j_\varsigma} V_{j_\varsigma l_\varsigma}^{-1}. \end{aligned} \quad (60)$$

A solution of the integral in Eq. (59) can be obtained using Cauchy's residue calculus [57, Chapter 6]. Let $\mathbb{H} = \{z \in \mathbb{C} \mid \text{Im}(z) > 0\}$ denote the upper half-plane of the

complex plane and $\overline{\mathbb{H}} = \mathbb{H} \cup \mathbb{R}$ its closure. We consider a function I , which is holomorphic in $\overline{\mathbb{H}}$ apart from finitely many points which do not lie on the real axis. We further assume that the integral $\mathcal{I} = \int_{-\infty}^{\infty} I(x) dx$ exists and $\lim_{z \rightarrow \infty} zI(z) = 0$. Then Cauchy's contour can be closed in the upper half-plane $\mathbb{H} = \{z \in \mathbb{C} \mid \text{Im}(z) > 0\}$.



As a consequence of Cauchy's residue theorem, the improper integral can be written as [57]

$$\mathcal{I} = 2\pi i \sum_{a \in \mathbb{H}} \text{ind}_{\Gamma}(a) \text{res}_a I, \quad (61)$$

where $\text{ind}_{\Gamma}(a)$ is the winding number, which equals one for all poles and our specifically chosen integration contour $\Gamma(r)$. For a proof, the limit $r \rightarrow \infty$ is taken and the complex periphery part is assessed by means of $\lim_{z \rightarrow \infty} zI(z) = 0$. Further note that, for poles of order one, the residues can be calculated by [57]

$$\text{res}_a I = \lim_{\omega \rightarrow a} (\omega - a) I(\omega). \quad (62)$$

In the following two sections, we consider two popular response functions in neuroscience. Explicit results for loops with two or three edges are given.

3.2.1 Example I: exponential-decay response function

For an exponentially decaying response function h

$$h(t) = \frac{1}{\tau} e^{-t/\tau} \Theta(t), \quad (63)$$

the Fourier transform is

$$\widehat{h}(\omega) = \frac{1}{(1 + i\tau\omega)}. \quad (64)$$

Thus, the elementary components D_i in Eq. (57) of the integrand I of \mathcal{I} from Eq. (59) are given by

$$D_i^e(\omega) = \frac{1}{1 + i\tau\omega - \xi_i}. \quad (65)$$

Explicit calculus yields the following expressions for k -point integrals. This terminology specifies the number of loop edges to be k .

Two-point integral The two-point integral with two loop edges reads

$$\mathcal{I}_{i,j}^e(\omega_0) = \int_{-\infty}^{\infty} D_i^e(\omega_0 - \omega) D_j^e(\omega) d\omega, \quad (66)$$

and its integrand $I_{i,j}^e$ has (up to) two poles in \mathbb{H}

$$a^{(i)} = \frac{i}{\tau} (\xi_i - 1) + \omega_0, \quad (67)$$

$$a^{(j)} = -\frac{i}{\tau} (\xi_j - 1). \quad (68)$$

The residues obtained from Eq. (62) are

$$\text{res}_{a^{(i)}} I_{i,j}^e = \frac{i}{\tau} D_j^e(a^{(i)}), \quad (69)$$

$$\text{res}_{a^{(j)}} I_{i,j}^e = -\frac{i}{\tau} D_i^e(\omega_0 - a^{(j)}). \quad (70)$$

The integral $\mathcal{I}_{i,j}^e(\omega_0)$ is then given by Eq. (61). Assuming $\text{Re } \xi_i < 1$ for all $i \in \{1, \dots, n\}$, only the pole $a^{(j)}$ lies in the upper half-plane and the integral explicitly reads

$$\mathcal{I}_{i,j}^e(\omega_0) = \frac{2\pi}{\tau} (2 - \xi_i - \xi_j + i\tau\omega_0)^{-1}. \quad (71)$$

The assumption $\text{Re } \xi_i < 1$ for all $i \in \{1, \dots, n\}$ is made for simplicity. If it does not hold, the poles inside the contour might be different, and the sum over residues in Eq. (61) has to be evaluated accordingly. In the case that poles are on the real axis, as it is the case if $\text{Re } \xi_i = 1$, perturbing the poles by $\pm i\varepsilon$ for some small $\varepsilon > 0$, performing the integration, and then taking the limit $\varepsilon \rightarrow 0$, yields the desired result.

Three-point integral If the loop has three edges, there are two integrals to be solved. The integrand of the first integral,

$$\mathcal{I}_{i,jk}^e(\omega_0, \nu_1) = \int_{-\infty}^{\infty} D_i^e(\omega_0 - \omega) D_j^e(\omega) D_k^e(\nu_1 + \omega) d\omega, \quad (72)$$

has poles

$$a^{(i)} = \frac{i}{\tau} (\xi_i - 1) + \omega_0, \quad (73)$$

$$a^{(j)} = -\frac{i}{\tau} (\xi_j - 1), \quad (74)$$

$$a^{(k)} = -\frac{i}{\tau} (\xi_k - 1) - \nu_1. \quad (75)$$

The residues in these poles are

$$\text{res}_{a^{(i)}} I_{i,jk}^e = \frac{i}{\tau} D_j^e(a^{(i)}) D_k^e(\nu_1 + a^{(i)}), \quad (76)$$

$$\text{res}_{a^{(j)}} I_{i,jk}^e = -\frac{i}{\tau} D_i^e(\omega_0 - a^{(j)}) D_k^e(\nu_1 + a^{(j)}), \quad (77)$$

$$\text{res}_{a^{(k)}} I_{i,jk}^e = -\frac{i}{\tau} D_i^e(\omega_0 - a^{(k)}) D_j^e(a^{(k)}). \quad (78)$$

The other possible three-point integral,

$$\mathcal{I}_{ij,k}^e(\omega_0, \omega_1) = \int_{-\infty}^{\infty} D_i^e(\omega_0 - \omega) D_j^e(\omega_1 - \omega) D_k^e(\omega) d\omega \quad (79)$$

has an integrand $I_{ij,k}^e$ with poles

$$a^{(i)} = \frac{i}{\tau} (\xi_i - 1) + \omega_0, \quad (80)$$

$$a^{(j)} = \frac{i}{\tau} (\xi_j - 1) + \omega_1, \quad (81)$$

$$a^{(k)} = -\frac{i}{\tau} (\xi_k - 1), \quad (82)$$

and corresponding residues

$$\text{res}_{a^{(i)}} I_{ij,k}^e = \frac{i}{\tau} D_j^e(\omega_1 - a^{(i)}) D_k^e(a^{(i)}), \quad (83)$$

$$\text{res}_{a^{(j)}} I_{ij,k}^e = \frac{i}{\tau} D_i^e(\omega_0 - a^{(j)}) D_k^e(a^{(j)}), \quad (84)$$

$$\text{res}_{a^{(k)}} I_{ij,k}^e = -\frac{i}{\tau} D_i^e(\omega_0 - a^{(k)}) D_j^e(\omega_1 - a^{(k)}). \quad (85)$$

The analytic form of the integrals $\mathcal{I}_{i,jk}^e(\omega_0, \nu_1)$ and $\mathcal{I}_{ij,k}^e(\omega_0, \omega_1)$ is again given by Eq. (61) and greatly simplifies when assuming $\text{Re } \xi_i < 1$ for all $i \in \{1, \dots, n\}$.

3.2.2 Example II: α -type response function

Another commonly used response function h is given by

$$h(t) = \frac{t}{\tau^2} e^{-t/\tau} \Theta(t), \quad (86)$$

where the Fourier transform reads

$$\widehat{h}(\omega) = \frac{1}{(1 + i\tau\omega)^2}. \quad (87)$$

This specific form is used for modeling synaptic interactions [58, 59] and is usually called α -function in a neuroscientific context. We adopt this terminology in the following. For the α -type response function, the elementary components D_i of the integrand I read

$$D_i^\alpha(\omega) = \frac{1}{(1 + i\tau\omega)^2 - \xi_i}. \quad (88)$$

Similar to the previous section, some results are stated explicitly.

Two-point integral Given α -type response functions, the integral of Eq. (59) reads

$$\mathcal{I}_{i,j}^\alpha(\omega_0) = \int_{-\infty}^{\infty} D_i^\alpha(\omega_0 - \omega) D_j^\alpha(\omega) d\omega. \quad (89)$$

The integrand $I_{i,j}^\alpha$ of $\mathcal{I}_{i,j}^\alpha$ has four poles,

$$a_\pm^{(i)} = \frac{i}{\tau} \left(\pm \sqrt{\xi_i} - 1 \right) + \omega_0, \quad (90)$$

$$a_\pm^{(j)} = -\frac{i}{\tau} \left(\pm \sqrt{\xi_j} - 1 \right). \quad (91)$$

The corresponding residues are given by

$$\text{res}_{a_\pm^{(i)}} I_{i,j}^\alpha = \pm \frac{i}{2\tau\sqrt{\xi_i}} D_j^\alpha \left(a_\pm^{(i)} \right), \quad (92)$$

$$\text{res}_{a_\pm^{(j)}} I_{i,j}^\alpha = \mp \frac{i}{2\tau\sqrt{\xi_j}} D_i^\alpha \left(\omega_0 - a_\pm^{(j)} \right). \quad (93)$$

Summing up residues while assuming $|\text{Re}(\sqrt{\xi_i})| < 1$ for all $i \in \{1, \dots, n\}$ as discussed above, yields the analytical expression

$$\mathcal{I}_{i,j}^\alpha(\omega_0) = \frac{\pi}{\tau\sqrt{\xi_j}} \left(D_i^\alpha \left(\omega_0 - a_+^{(j)} \right) - D_i^\alpha \left(\omega_0 - a_-^{(j)} \right) \right). \quad (94)$$

Three-point integral As for exponential response functions, a loop with three edges occurs in two variants

$$\mathcal{I}_{i,jk}^\alpha(\omega_0, \nu_1) = \int_{-\infty}^{\infty} D_i^\alpha(\omega_0 - \omega) D_j^\alpha(\omega) D_k^\alpha(\nu_1 + \omega) d\omega, \quad (95)$$

and

$$\mathcal{I}_{ij,k}^\alpha(\omega_0, \omega_1) = \int_{-\infty}^{\infty} D_i^\alpha(\omega_0 - \omega) D_j^\alpha(\omega_1 - \omega) D_k^\alpha(\omega) d\omega. \quad (96)$$

The poles and residues are deduced analogously and are omitted at this point.

3.3 Explicit predictions

The general loop integrals derived in Section 3.2 can now be used to obtain approximations for cumulants of any order. First we have a closer look at the motivating example from the beginning of this section. Afterwards, the one-loop correction to the second-order cumulant is calculated.

3.3.1 One-loop correction to the rates

As stated earlier in Eq. (41), the working point \bar{r} of our series expansion of the nonlinearity corresponds to the tree-level expectation value. This means

$$\langle \delta z_i \rangle_T = 0 \quad \forall i \in \{1, \dots, n\}, \quad (97)$$

and the working point is determined by solving the self-consistency equation

$$\bar{r}_i(t) = \phi \left(\sum_j (h_{ij} \star \bar{r}_j)(t) + b_i(t) \right). \quad (98)$$

If we want to know how the tree-level covariances influence the rates, we have to calculate the one-loop correction

$$\begin{aligned} \langle \delta z_i \rangle_{1\text{-loop}} &= \text{Diagram} \\ &= 2 \cdot \sum_{j,l} \int \Delta_{T,ij}(t, t_1) \frac{\phi_j^{(2)}}{1!2!} (h \star_1 \Delta_T)_{jl}(t_1, t_2) (h \star_1 \Delta_T)_{jl}(t_1, t_2) \\ &\quad \times \frac{\phi_l^{(0)}}{2!} dt_2 dt_1. \end{aligned}$$

According to the Feynman rules in Section 2.2.1, there is only a single diagram contributing. For a strict-sense stationary process, the propagator only depends on the time difference, $\Delta_T(t_1, t_2) = \Delta_T(t_1 - t_2)$. This yields the Fourier representation

$$\Delta_T(t_1 - t_2) = \frac{1}{2\pi} \int \hat{\Delta}_T(\omega) e^{i\omega(t_1 - t_2)} d\omega, \quad (99)$$

and thus

$$\begin{aligned} (h \star_1 \Delta_T)_{jl}(t_1 - t_2) &= \frac{1}{2\pi} \int \sum_m \hat{h}_{jm}(\omega) \hat{\Delta}_{T,ml}(\omega) e^{i\omega(t_1 - t_2)} d\omega \\ &= \frac{1}{2\pi} \int E_{jl}(\omega) e^{i\omega(t_1 - t_2)} d\omega. \end{aligned} \quad (100)$$

Using this Fourier representation of loop edges, one gets

$$\begin{aligned} \langle \delta z_i \rangle_{1\text{-loop}} &= \frac{1}{2} \frac{1}{(2\pi)^3} \int \sum_{j,l} \hat{\Delta}_{T,ij}(\omega_1) E_{jl}(\omega_2) E_{jl}(\omega_3) \phi_j^{(2)} \phi_l^{(0)} \\ &\quad \times e^{i\omega_1(t-t_1)} e^{i\omega_2(t_1-t_2)} e^{i\omega_3(t_1-t_2)} d\omega_3 d\omega_2 d\omega_1 dt_2 dt_1. \end{aligned} \quad (101)$$

The time integrals yield δ -functions, such that

$$\begin{aligned} \langle \delta z_i \rangle_{1\text{-loop}} &= \frac{1}{4\pi} \int \sum_{j,l} \hat{\Delta}_{T,ij}(\omega_1) E_{jl}(\omega_2) E_{jl}(\omega_3) \phi_j^{(2)} \phi_l^{(0)} \\ &\quad \times e^{i\omega_1 t} \delta(\omega_1 - \omega_2 - \omega_3) \delta(\omega_2 + \omega_3) d\omega_3 d\omega_2 d\omega_1 \\ &= \frac{1}{4\pi} \int \sum_{j,l} \hat{\Delta}_{T,ij}(0) E_{jl}(-\omega_3) E_{jl}(\omega_3) \phi_j^{(2)} \phi_l^{(0)} d\omega_3. \end{aligned} \quad (102)$$

In the last step, the ω_1 - and ω_2 -integrations over the δ -functions are performed.

With the shorthand from Eq. (53), the final result reads

$$\langle \delta z_i \rangle_{1\text{-loop}} = \frac{1}{4\pi} \sum_{j,l} \hat{\Delta}_{T,ij}(0) \mathcal{L}_{jl,jl}(0) \phi_j^{(2)} \phi_l^{(0)}. \quad (103)$$

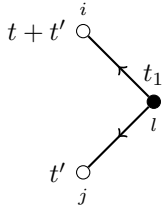
Thus, in total, the one-loop correction to the rates arising from the nonlinearity depends on the steady-state rate vector and the second derivative of the nonlinear gain function evaluated at the steady-state rate vector. Further, the simplest loop integral $\mathcal{L}_{jl,jl}(0)$ and the tree-level propagator contribute.

3.3.2 One-loop correction to the covariance

The covariance of the two spike trains z_i and z_j is given by

$$C_{ij}(t + t', t') = \langle \delta z_i(t + t') \delta z_j(t') \rangle. \quad (104)$$

By means of the Feynman rules described in Section 2.2.1, the tree-level covariance can thus be deduced from the following diagram

$$C_{ij}^{\text{tree}}(t + t', t') =$$


$$= 2 \cdot \sum_k \int \Delta_{T,ik}(t + t', t_1) \frac{\phi_k^{(0)}}{2!} \Delta_{T,jk}(t', t_1) dt_1. \quad (105)$$

Considering again a strict-sense stationary process, the Fourier-transformed result reads

$$\widehat{C}_{ij}^{\text{tree}}(\omega) = \sum_k \widehat{\Delta}_{T,ik}(\omega) \phi_k^{(0)} \widehat{\Delta}_{T,jk}(-\omega). \quad (106)$$

For linear mutually exciting point processes, this result matches the formula found by [16].

In case of non-vanishing second or third derivative of the nonlinear gain function at the working point, the one-loop correction to the covariance is nonzero. First, all contributing terms have to be identified. The following two-step procedure yields all Feynman diagrams with one loop and two external vertices. We start by creating all possible one-loop topologies, and then select the ones compatible with the Feynman rules from Section 2.2.1. As the loop characteristic determines the topology, we start with a simple circle and successively add legs and internal propagators to it. An additional line can be attached to each internal propagator or internal vertex. Internal vertices are only added to internal propagators between two vertices with more than three incoming or outgoing legs. This procedure terminates after finitely many iterations, because the order of the cumulant of interest limits the number of legs added, and the number of internal propagators between two vertices with more than three incoming or outgoing legs is finite. Once all topologies are created, the ones relevant for the LNP cascade model are identified. This leads to a set of

exactly 15 diagrams contributing to the second-order cumulant. The graphs whose contributions have to be calculated are given in Fig. 1, Fig. 2, and Fig. 3. Individual contributions are labeled by \mathcal{M}_{ij}^β with $\beta = 1, \dots, 15$.

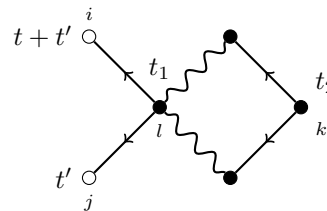
The one-loop covariance correction is given by the sum over all contributions from the distinct diagrams

$$C_{ij}^{1\text{-loop}}(t+t', t') = \sum_{\beta=1}^{15} \mathcal{M}_{ij}^\beta(t+t', t'). \quad (107)$$

The authors of [30] considered only a subset of these terms, namely \mathcal{M}_{ij}^β for $\beta \in \{1, \dots, 5\}$. The remaining 10 contributions ($\beta = 6, \dots, 15$) were neglected by these authors. However, these diagrams contain one loop and must be taken into account. Remember that the contributions of higher-order fluctuations are directly reflected by the number of loops in the diagrams [30, 55]. The method used in [30] to construct the loop diagrams for the covariance correction (cf. Fig. 13 in their article) was imperfect, though. An algorithm for the automated generation of Feynman diagrams is proposed in the discussion section of this article.

The individual contributions to the one-loop correction of the covariance in Eq. (107) are solved independently. The procedure is illustrated for the \mathcal{M}_{ij}^1 component. For all other contributions we only list the result.

Translating the Feynman diagram into formula yields

$$\begin{aligned} \mathcal{M}_{ij}^1(t+t', t') &= \text{Diagram} \\ &= 4 \cdot \int \sum_{l,k} \Delta_{T,il}(t+t', t_1) \Delta_{T,jl}(t', t_1) \frac{\phi_l^{(2)}}{2!2!} \\ &\quad \times (h \star_1 \Delta_T)_{lk}(t_1, t_2) (h \star_1 \Delta_T)_{lk}(t_1, t_2) \frac{\phi_k^{(0)}}{2!} dt_1 dt_2. \end{aligned} \quad (108)$$


Considering again a strict-sense stationary process, the covariance only depends on the time lag t , and the reference time t' can be chosen arbitrarily. Also the propagator depends only on the time difference and has the Fourier representation (99).

Choosing $t' = 0$ and using Eq. (100) results in

$$\begin{aligned} \mathcal{M}_{ij}^1(t) = & \frac{1}{2} \frac{1}{(2\pi)^4} \int \sum_{l,k} \hat{\Delta}_{T,il}(\omega_1) \hat{\Delta}_{T,jl}(\omega_2) E_{lk}(\omega_3) E_{lk}(\omega_4) \phi_l^{(2)} \phi_k^{(0)} \\ & \times e^{i\omega_1(t-t_1)} e^{-i\omega_2 t_1} e^{i\omega_3(t_1-t_2)} e^{i\omega_4(t_1-t_2)} d\omega_4 d\omega_3 d\omega_2 d\omega_1 dt_2 dt_1. \end{aligned} \quad (109)$$

The time integrals yield δ -functions such that

$$\begin{aligned} \mathcal{M}_{ij}^1(t) = & \frac{1}{2} \frac{1}{(2\pi)^2} \int \sum_{l,k} \hat{\Delta}_{T,il}(\omega_1) \hat{\Delta}_{T,jl}(\omega_2) E_{lk}(\omega_3) E_{lk}(\omega_4) \phi_l^{(2)} \phi_k^{(0)} \\ & \times e^{i\omega_1 t} \delta(\omega_1 + \omega_2 - \omega_3 - \omega_4) \delta(\omega_3 + \omega_4) d\omega_4 d\omega_3 d\omega_2 d\omega_1. \end{aligned} \quad (110)$$

Executing the ω_2 - and ω_4 -integrations leads to

$$\begin{aligned} \mathcal{M}_{ij}^1(t) = & \frac{1}{2} \frac{1}{(2\pi)^2} \int \sum_{l,k} \hat{\Delta}_{T,il}(\omega_1) \hat{\Delta}_{T,jl}(-\omega_1) E_{lk}(\omega_3) E_{lk}(-\omega_3) \\ & \times \phi_l^{(2)} \phi_k^{(0)} e^{i\omega_1 t} d\omega_3 d\omega_1 \\ = & \frac{1}{2\pi} \int \frac{1}{4\pi} \sum_{l,k} \hat{\Delta}_{T,il}(\omega_1) \hat{\Delta}_{T,jl}(-\omega_1) \mathcal{L}_{lk,lk}(0) \phi_l^{(2)} \phi_k^{(0)} e^{i\omega_1 t} d\omega_1. \end{aligned} \quad (111)$$

The contribution of the first diagram to the coherence between neuron i and j thus reads

$$\widehat{\mathcal{M}}_{ij}^1(\omega) = \frac{1}{4\pi} \sum_{l,k} \hat{\Delta}_{T,il}(\omega) \hat{\Delta}_{T,jl}(-\omega) \mathcal{L}_{lk,lk}(0) \phi_l^{(2)} \phi_k^{(0)} \quad (112)$$

where we use our loop integral abbreviations (53).

The other contributions are derived similarly and the resulting terms read

$$\widehat{\mathcal{M}}_{ij}^2(\omega) = \frac{1}{4\pi} \sum_{l,k} \hat{\Delta}_{T,ik}(\omega) \hat{\Delta}_{T,jl}(-\omega) \mathcal{L}_{lk,lk}(-\omega) \phi_l^{(2)} \phi_k^{(0)}, \quad (113)$$

$$\begin{aligned} \widehat{\mathcal{M}}_{ij}^3(\omega) = & \frac{1}{4\pi} \sum_{l,k} \hat{\Delta}_{T,il}(\omega) \hat{\Delta}_{T,jk}(-\omega) \mathcal{L}_{lk,lk}(\omega) \phi_l^{(2)} \phi_k^{(0)} \\ = & \widehat{\mathcal{M}}_{ji}^2(-\omega), \end{aligned} \quad (114)$$

$$\widehat{\mathcal{M}}_{ij}^4(\omega) = \frac{1}{4\pi} \sum_{l,k,m} \hat{\Delta}_{T,il}(\omega) \hat{\Delta}_{T,jm}(-\omega) \mathcal{L}_{lk,lk}(\omega) E_{km}(\omega) \phi_l^{(2)} \phi_k^{(1)} \phi_m^{(0)}, \quad (115)$$

$$\begin{aligned}\widehat{\mathcal{M}}_{ij}^5(\omega) &= \frac{1}{4\pi} \sum_{l,k,m} \widehat{\Delta}_{T,im}(\omega) \widehat{\Delta}_{T,jl}(-\omega) \mathcal{L}_{lk,lk}(-\omega) E_{km}(-\omega) \phi_l^{(2)} \phi_k^{(1)} \phi_m^{(0)} \\ &= \widehat{\mathcal{M}}_{ji}^4(-\omega),\end{aligned}\quad (116)$$

$$\widehat{\mathcal{M}}_{ij}^6(\omega) = \frac{1}{4\pi} \sum_{l,k,m} \widehat{\Delta}_{T,il}(\omega) \widehat{\Delta}_{T,jk}(-\omega) \mathcal{L}_{lm,lkm}(0, \omega) \phi_l^{(2)} \phi_k^{(1)} \phi_m^{(0)}, \quad (117)$$

$$\widehat{\mathcal{M}}_{ij}^7(\omega) = \frac{1}{4\pi} \sum_{l,k,m} \widehat{\Delta}_{T,ik}(\omega) \widehat{\Delta}_{T,jl}(-\omega) \mathcal{L}_{lkm,lm}(-\omega, 0) \phi_l^{(2)} \phi_k^{(1)} \phi_m^{(0)}, \quad (118)$$

$$\widehat{\mathcal{M}}_{ij}^8(\omega) = \frac{1}{4\pi} \sum_{m,l,k} \widehat{\Delta}_{T,im}(\omega) \widehat{\Delta}_{T,jm}(-\omega) E_{mk}(0) \mathcal{L}_{kl,kl}(0) \phi_m^{(1)} \phi_k^{(2)} \phi_l^{(0)}, \quad (119)$$

$$\widehat{\mathcal{M}}_{ij}^9(\omega) = \frac{1}{4\pi} \sum_{k,l,m} \widehat{\Delta}_{T,im}(\omega) \widehat{\Delta}_{T,jk}(-\omega) E_{km}(-\omega) \mathcal{L}_{kl,kl}(0) \phi_k^{(3)} \phi_l^{(0)} \phi_m^{(0)}, \quad (120)$$

$$\begin{aligned}\widehat{\mathcal{M}}_{ij}^{10}(\omega) &= \frac{1}{4\pi} \sum_{k,l,m} \widehat{\Delta}_{T,ik}(\omega) \widehat{\Delta}_{T,jm}(-\omega) E_{km}(\omega) \mathcal{L}_{kl,kl}(0) \phi_k^{(3)} \phi_l^{(0)} \phi_m^{(0)} \\ &= \widehat{\mathcal{M}}_{ji}^9(-\omega),\end{aligned}\quad (121)$$

$$\begin{aligned}\widehat{\mathcal{M}}_{ij}^{11}(\omega) &= \frac{1}{8\pi} \sum_{k,l,m,p} \widehat{\Delta}_{T,ip}(\omega) \widehat{\Delta}_{T,jk}(-\omega) \mathcal{L}_{klm,km}(-\omega, 0) E_{lp}(-\omega) \\ &\quad \times \phi_k^{(2)} \phi_l^{(2)} \phi_m^{(0)} \phi_p^{(0)},\end{aligned}\quad (122)$$

$$\begin{aligned}\widehat{\mathcal{M}}_{ij}^{12}(\omega) &= \frac{1}{8\pi} \sum_{k,l,m,p} \widehat{\Delta}_{T,ik}(\omega) \widehat{\Delta}_{T,jp}(-\omega) \mathcal{L}_{km,klm}(0, \omega) E_{lp}(\omega) \\ &\quad \times \phi_k^{(2)} \phi_l^{(2)} \phi_m^{(0)} \phi_p^{(0)},\end{aligned}\quad (123)$$

$$\begin{aligned}\widehat{\mathcal{M}}_{ij}^{13}(\omega) &= \frac{1}{16\pi} \sum_{k,l,m,p} \widehat{\Delta}_{T,ik}(\omega) \widehat{\Delta}_{T,jp}(-\omega) E_{kp}(\omega) E_{kl}(0) \mathcal{L}_{lm,lm}(0) \\ &\quad \times \phi_k^{(2)} \phi_l^{(2)} \phi_m^{(0)} \phi_p^{(0)},\end{aligned}\quad (124)$$

$$\begin{aligned}
\widehat{\mathcal{M}}_{ij}^{14}(\omega) &= \frac{1}{16\pi} \sum_{k,l,m,p} \widehat{\Delta}_{T,ip}(\omega) \widehat{\Delta}_{T,jk}(-\omega) E_{kp}(-\omega) E_{kl}(0) \mathcal{L}_{lm,lm}(0) \\
&\quad \times \phi_k^{(2)} \phi_l^{(2)} \phi_m^{(0)} \phi_p^{(0)} \\
&= \widehat{\mathcal{M}}_{ji}^{13}(-\omega),
\end{aligned} \tag{125}$$

$$\begin{aligned}
\widehat{\mathcal{M}}_{ij}^{15}(\omega) &= \frac{1}{8\pi} \sum_{k,l,m,p} \widehat{\Delta}_{T,ik}(\omega) \widehat{\Delta}_{T,jl}(-\omega) \phi_k^{(2)} \phi_l^{(2)} \phi_m^{(0)} \phi_p^{(0)} \\
&\quad \times \int E_{kp}(-\omega') E_{km}(\omega + \omega') E_{lm}(-\omega - \omega') E_{lp}(\omega') d\omega'.
\end{aligned} \tag{126}$$

For the comparison with data, it is convenient to work with the integrated cross-covariances

$$c_{ij} = \int_{-\infty}^{\infty} C_{ij}(t) dt. \tag{127}$$

Note that $c_{ij} = \widehat{C}_{ij}(0)$ with \widehat{C} denoting the cross-spectra. We get this quantity directly by adding up all contributions from the previously listed terms evaluated at $\omega = 0$. The one-loop correction thus reads

$$c_{ij}^{1-\text{loop}} = \sum_{\beta=1}^{15} \widehat{\mathcal{M}}_{ij}^{\beta}(0). \tag{128}$$

For a prediction of the one-loop correction to the integrated covariance, the only loop integrals to be calculated from this general class are $\mathcal{L}_{lk,lk}(0)$, $\mathcal{L}_{lm,lkm}(0,0)$, and $\mathcal{L}_{lkm,lm}(0,0)$. The simplest integral involved in the one-loop correction to the first- or second-order cumulant is $\mathcal{L}_{lk,lk}(0)$ which is solely based on $\mathcal{I}_{i,j}(0)$ from Eq. (59). Let ξ_i denote the i -th eigenvalue of $D_{\phi(1)}W$, as described previously. Assuming for simplicity $\text{Re } \xi_i < 1$ for all $i \in \{1, \dots, n\}$ (see remark in Section 3.2.1), the integral with exponentially decaying response function reads (cf. Eq. (71))

$$\mathcal{I}_{i,j}^e(0) = \frac{2\pi}{\tau} (2 - \xi_i - \xi_j)^{-1}. \tag{129}$$

For an α -shaped response function, we assume $|\text{Re}(\sqrt{\xi_i})| < 1$ for all $i \in \{1, \dots, n\}$ and obtain from Eq. (94)

$$\mathcal{I}_{i,j}^{\alpha}(0) = \frac{\pi}{\tau \sqrt{\xi_j}} \left(D_i^{\alpha} \left(-a_+^{(j)} \right) - D_i^{\alpha} \left(-a_-^{(j)} \right) \right), \tag{130}$$

with $D_i^\alpha(\omega)$ from Eq. (88). This simplifies to

$$\mathcal{I}_{i,j}^\alpha(0) = \frac{8\pi}{\tau} \left(\xi_j^2 + (\xi_i - 4)^2 - 2\xi_j(4 + \xi_i) \right)^{-1}. \quad (131)$$

Putting everything together, we obtain

$$\mathcal{L}_{lk,lk}^e(0) = \frac{2\pi}{\tau} \sum_{i,j=1}^n (WV)_{li} V_{ik}^{-1} (WV)_{lj} V_{jk}^{-1} (2 - \xi_i - \xi_j)^{-1} \quad (132)$$

for the exponentially decaying response function, and

$$\mathcal{L}_{lk,lk}^\alpha(0) = \frac{8\pi}{\tau} \sum_{i,j=1}^n (WV)_{li} V_{ik}^{-1} (WV)_{lj} V_{jk}^{-1} \left(\xi_j^2 + (\xi_i - 4)^2 - 2\xi_j(4 + \xi_i) \right)^{-1} \quad (133)$$

for the α -type response function.

For vanishing frequencies, the two three-point loop integrals $\mathcal{L}_{lm,lkm}(0,0)$ and $\mathcal{L}_{lkm,lm}(0,0)$ coincide. This can be seen by performing a transformation of the integration variable, $\omega \rightarrow -\omega'$, in the integral $\mathcal{I}_{i_0 i_1, j_0}(0,0)$ from Eq. (59), which results in

$$\mathcal{I}_{i_0 i_1, j_0}(0,0) = \mathcal{I}_{j_0, i_0 i_1}(0,0). \quad (134)$$

If we assume again that all eigenvalues ξ_i ($i = 1, \dots, n$) of $D_{\phi(1)}W$ have a real part strictly smaller than one, the integral with exponentially decaying response function reads

$$\mathcal{I}_{i_0 i_1, j_0}^e = \frac{2\pi}{\tau} (2 - \xi_{j_0} - \xi_{i_0})^{-1} (2 - \xi_{j_0} - \xi_{i_1})^{-1}. \quad (135)$$

This results in

$$\begin{aligned} \mathcal{L}_{lm,lkm}^e(0,0) = \mathcal{L}_{lkm,lm}^e(0,0) &= \sum_{i_0, i_1, j_0=1}^n (WV)_{li_0} V_{i_0 k}^{-1} (WV)_{ki_1} V_{i_1 m}^{-1} \\ &\quad \times (WV)_{lj_0} V_{j_0 m}^{-1} \mathcal{I}_{i_0 i_1, j_0}^e. \end{aligned} \quad (136)$$

Assuming $|\operatorname{Re}(\sqrt{\xi_i})| < 1$ and $\xi_i \neq 0$ for all $i \in \{1, \dots, n\}$, the integral with α -type response function is given by

$$\begin{aligned} \mathcal{I}_{i_0 i_1, j_0}^\alpha = \frac{\pi}{\tau \sqrt{\xi_{j_0}}} & \left(\left(\left(2 - \sqrt{\xi_{j_0}} \right)^2 - \xi_{i_0} \right)^{-1} \left(\left(2 - \sqrt{\xi_{j_0}} \right)^2 - \xi_{i_1} \right)^{-1} \right. \\ & \left. - \left(\left(2 + \sqrt{\xi_{j_0}} \right)^2 - \xi_{i_0} \right)^{-1} \left(\left(2 + \sqrt{\xi_{j_0}} \right)^2 - \xi_{i_1} \right)^{-1} \right). \end{aligned} \quad (137)$$

This results in the complete loop integral

$$\begin{aligned} \mathcal{L}_{lm, lkm}^\alpha(0, 0) = \mathcal{L}_{lkm, lm}^\alpha(0, 0) = \sum_{i_0, i_1, j_0=1}^n & (WV)_{li_0} V_{i_0 k}^{-1} (WV)_{ki_1} V_{i_1 m}^{-1} \\ & \times (WV)_{lj_0} V_{j_0 m}^{-1} \mathcal{I}_{i_0 i_1, j_0}^\alpha. \end{aligned} \quad (138)$$

The one-loop correction \mathcal{M}^{15} contains a loop integral differing from the general class of Eq. (53). However, it can be reduced to an integral $\mathcal{I}_{i_0 i_1, j_0 j_1}$ from Eq. (59). Note that one has

$$\begin{aligned} \int E_{kp}(-\omega') E_{lm}(-\omega - \omega') E_{lp}(\omega') E_{km}(\omega + \omega') d\omega' = \\ \sum_{i_0, i_1, j_0, j_1} (WV)_{ki_0} V_{i_0 p}^{-1} (WV)_{li_1} V_{i_1 m}^{-1} (WV)_{lj_0} V_{j_0 p}^{-1} (WV)_{kj_1} V_{j_1 m}^{-1} \\ \times \underbrace{\int D_{i_0}(-\omega') D_{i_1}(-\omega - \omega') D_{j_0}(\omega') D_{j_1}(\omega + \omega') d\omega'}_{= \mathcal{I}_{i_0 i_1, j_0 j_1}(0, -\omega, \omega)}. \end{aligned} \quad (139)$$

Thus a solution can be obtained in a similar manner by the residue calculus.

To apply these results to the numerical simulations in Section 3.4, we need to calculate $\widehat{\mathcal{M}}^{15}(0)$ for the α -shaped response function. We thus need the analytic solution of $\mathcal{I}_{ij, kl}^\alpha(0, 0, 0)$. The integral reads

$$\mathcal{I}_{ij, kl}^\alpha(0, 0, 0) = \int D_i^\alpha(-\omega) D_j^\alpha(-\omega) D_k^\alpha(\omega) D_l^\alpha(\omega) d\omega, \quad (140)$$

and assuming $|\operatorname{Re}(\sqrt{\xi_i})| < 1$, the factors D_k^α and D_l^α cause poles of the integrand in the upper half-plane. Two cases have to be distinguished. We either have $\xi_k \neq \xi_l$

or $\xi_k = \xi_l$. In the former case, the relevant poles are

$$a_{\pm}^{(k)} = -\frac{i}{\tau} \left(\pm \sqrt{\xi_k} - 1 \right), \quad (141)$$

$$a_{\pm}^{(l)} = -\frac{i}{\tau} \left(\pm \sqrt{\xi_l} - 1 \right), \quad (142)$$

and the residues of the integrand $I_{ij,kl}^{\alpha}$ are given by

$$\text{res}_{a_{\pm}^{(k)}} I_{ij,kl}^{\alpha} = \pm \frac{1}{2i\tau\sqrt{\xi_k}} \frac{1}{\xi_k - \xi_l} \left(\left(2 \mp \sqrt{\xi_k} \right)^2 - \xi_i \right)^{-1} \left(\left(2 \mp \sqrt{\xi_k} \right)^2 - \xi_j \right)^{-1}, \quad (143)$$

$$\text{res}_{a_{\pm}^{(l)}} I_{ij,kl}^{\alpha} = \pm \frac{1}{2i\tau\sqrt{\xi_l}} \frac{1}{\xi_l - \xi_k} \left(\left(2 \mp \sqrt{\xi_l} \right)^2 - \xi_i \right)^{-1} \left(\left(2 \mp \sqrt{\xi_l} \right)^2 - \xi_j \right)^{-1}. \quad (144)$$

In the latter case, where $\xi_l = \xi_k$, the poles $a_{\pm}^{(k)} = -\frac{i}{\tau} (\pm \sqrt{\xi_k} - 1)$ are of order two.

The residues are given by

$$\begin{aligned} \text{res}_{a_{\pm}^{(k)}} I_{ij,kl}^{\alpha} &= \frac{-i}{\tau} \left(\mp 4 + 8\xi_k^{\frac{3}{2}} \mp \frac{5}{4}\xi_k^2 + \sqrt{\xi_k}(16 - 2\xi_i - 2\xi_j) \pm \xi_i \left(1 - \frac{1}{4}\xi_j \right) \right. \\ &\quad \left. \mp \xi_k \left(18 - \frac{3}{4}\xi_i - \frac{3}{4}\xi_j \right) \pm \xi_j \right) \\ &\quad \times \xi_k^{-\frac{3}{2}} \left(\left(2 \mp \sqrt{\xi_k} \right)^2 - \xi_i \right)^{-2} \left(\left(2 \mp \sqrt{\xi_k} \right)^2 - \xi_j \right)^{-2}. \end{aligned} \quad (145)$$

The final integral is given by summing up the residues according to Eq. (61) and inserting the result into Eq. (139) evaluated at $\omega = 0$.

3.4 Numerical results

This section provides a worked example for how loop corrections can improve cumulant predictions in the LNP cascade model. The results from Section 3.3 are compared to a simulation of the process. An outstanding feature of the theory are cumulant predictions for individual neurons, rather than population-averaged quantities. We would like to stress this by looking at predictions for individual neurons or pairs of neurons resulting in predictions of full distributions for the respective cumulants in the network, rather than just mean values.

3.4.1 Statistical measures

In order to compare our predictions, corresponding quantities have to be extracted from the simulated spike trains. In particular, the mean firing rate of a neuron is

estimated by

$$\check{\lambda}_i = \frac{\check{N}_i(\Delta)}{\Delta}, \quad (146)$$

where $\check{N}_i(\Delta)$ is the number of spikes in a time window of length Δ . Estimated quantities are marked with “ $\check{\cdot}$ ” throughout this section, to distinguish them from theoretical ones. The integrated second-order cumulant $c_{ij} = \int_{-\infty}^{\infty} C_{ij}(t) dt = \hat{C}_{ij}(0)$, for simplicity denoted as covariance in the following, is estimated according to

$$\check{c}_{ij} = \lim_{\Delta \rightarrow \infty} \frac{\text{Cov}[\check{N}_i(\Delta), \check{N}_j(\Delta)]}{\Delta}. \quad (147)$$

If we talk about cross-covariance in the following, we explicitly mean off-diagonal terms of this matrix ($i \neq j$). Auto-covariances are the diagonal elements ($i = j$).

3.4.2 Simulation parameters

For numerical comparison, we simulate a two-population network of $N = 250$ LNP neurons, which generate their spikes according to a Poisson distribution with conditional intensity (Eq. (12)),

$$\lambda_i(t) = \phi_i \left(\sum_j (h_{ij} \star z_j)(t) + b_i(t) \right). \quad (148)$$

The excitatory population comprises $N_E = 200$ and the inhibitory one $N_I = 50$ neurons. The adjacency matrix is an Erdős–Rényi graph with connection probability $p = 0.16$. The synaptic weights are given by $w_{EE} = 0.12$ for excitatory-excitatory connections, $w_{IE} = 0.1$ for excitatory-to-inhibitory connections, and $w_{EI} = w_{II} = -0.5$ for all inhibitory connections. The causal response function is chosen to be the α -function (defined in Eq. (86)) with synaptic time constant $\tau = 10$ ms. Aiming for non-trivial loop corrections, the nonlinear gain function is a rectified quadratic function for all nodes

$$\phi_i(x) = \Theta(x)x^2 \quad \forall i = 1, \dots, N. \quad (149)$$

The baseline firing rate corresponding to $\phi_i(b)$ is set to 10 Hz. The simulation time is $T = 2 \cdot 10^8$ ms with simulation time step of $\Delta t = 1$ ms. The simulation is implemented by the exact integration scheme outlined in [60]. For data analysis, the

first 10 s are dropped, and a spike count bin size of $\Delta_{\text{sc}} = 1000 \text{ ms}$ is used. The simulation was implemented in Python using the open-source software SciPy [61].

3.4.3 Rate predictions

The simulated stationary rates are compared to the theoretical predictions in Fig. 4. The tree-level prediction of the rates is given by \bar{r} from Eq. (98), corresponding to $\langle \delta z \rangle_T = 0$. The one-loop correction is given by Eq. (103), and the total one-loop prediction reads

$$r_i^{1-\text{loop}} = \bar{r}_i + \langle \delta z_i \rangle_{1-\text{loop}}. \quad (150)$$

Figure 4(a) compares tree-level predictions, and a larger discrepancy is observed for increasing rates. The one-loop prediction perfectly corrects for this mismatch and we observe nearly perfect agreement in Fig. 4(b).

The cumulative distribution function (cdf) of the rates is depicted in Fig. 5. The mean tree-level (one-loop) prediction of the rates is 11.7 Hz (12.5 Hz), and the estimated mean rate is 12.6 Hz. Excitatory neurons have a mean firing rate of 12.9 Hz (one-loop prediction), whereas for inhibitory ones the one-loop prediction is 10.8 Hz. Both values are in good agreement with the estimated population-specific mean rates 13.0 Hz and 10.9 Hz, respectively. The relative one-loop corrections range from 3.8 % to 21.2 %.

To better quantify the discrepancy, the residuals, i.e. the difference between predicted and estimated rate, is investigated. Figure 6 depicts the cdf of the residuals for the tree- and loop-level prediction. For the two-population model under consideration, we further split into excitatory and inhibitory groups. The one-loop correction yields a relevant reduction of the error in all cases. While the residuals have a broad range (from 0.39 Hz to 1.87 Hz) for tree-level predictions, the one-loop prediction corrects individual mismatches resulting in residuals ranging from 0.03 Hz to 0.13 Hz with a mean of 0.06 Hz.

3.4.4 Covariance predictions

Corrections arising from nonlinear gain functions are also calculated for the second-order cumulant of the process. The tree-level prediction is given by $c_{ij}^{\text{tree}} = \widehat{C}_{ij}^{\text{tree}}(0)$ from Eq. (106). For the full one-loop prediction, the one-loop correction $c_{ij}^{1-\text{loop}}$

obtained by Eq. (128) is added on top. Since the rectified quadratic nonlinearity ϕ has a vanishing third derivative, the contributions $\widehat{\mathcal{M}}^9$ and $\widehat{\mathcal{M}}^{10}$ are zero, cf. Eq. (120) and Eq. (121). All other terms yield nonzero corrections.

The mean of estimated cross-covariances is 0.4 Hz, which is small as compared to the mean of estimated auto-covariances at 14.1 Hz. The predicted tree-level cdf, the one-loop cdf, and the empirical cdf of the cross-covariance, respectively, are shown in Fig. 7(a), and the ones of the auto-covariance are depicted in Fig. 7(b). A very basic observation is that the auto-covariances are much larger than the cross-covariances. Because they roughly differ in one order of magnitude, we analyze the auto- and cross-covariance separately. This observation provides valuable insight and can inform new beyond-mean-field models. In the simulated network setting, the cross-covariance has a multimodal distribution. The one-loop correction improves the tree-level predictions for auto- and cross-covariances, as the one-loop cdf fits better to the estimated one. In both cases, we observe an almost perfect match between the one-loop prediction and the distribution of empirical covariances. Remarkably, the entire distribution is precisely predicted, and not just its mean.

For explicit comparison between simulation and prediction, the cdf of the residuals for all possible pairs of distinct neurons are shown in Fig. 8(a). While the distribution of cross-covariance residuals has a mean of 0.08 Hz with a standard deviation of 0.07 Hz for the tree-level prediction, the mean is 0.03 Hz for the one-loop predictions and the standard deviation slightly decreases to 0.04 Hz. In Fig. 8(b) the residuals for auto-covariance predictions are shown. Here, the improvement achieved by the additional one-loop corrections is even more pronounced due to the larger absolute values of auto-covariances compared to cross-covariances. The tree-level residual distribution has a mean of 1.02 Hz, whereas the mean of the one-loop residual distribution is 0.12 Hz. As obvious from Fig. 8(b), the standard deviation decreases drastically for residuals calculated with the one-loop predictions. This decrease in standard deviation clearly illustrates that the one-loop covariance corrections are specific for each pair of neurons. We stress once more that it is important to consider the entire distribution of residuals, because they can be either positive or negative. Therefore, the mean residual can be small, while the distribution spreads widely.

In total, we observe a remarkable improvement for second-order cumulant predictions. Both, the cross- and auto-covariance predictions get significantly closer

to the respective quantities extracted from a simulation of the process, if one-loop diagram contributions are taken into account.

4 Conclusions and Discussion

Predicting spike train cumulants in nonlinear spiking models is complicated by the fact that higher-order moments are coupling to lower-order ones. One approach is to expand the moment hierarchy in a series, where higher-order terms account for the influence of higher-order moments on the dynamics. Specifically, when representing the spiking activity in LNP cascade models by path integrals and appropriate path densities, one obtains a systematic series expansion for spike train cumulants. This series is called *loop expansion*, as the number of loops in the Feynman diagrams associated with the terms in the expansion reflect the successive contributions of higher-order fluctuations. For actual predictions the series expansion is truncated, ignoring contributions beyond the cutoff. In this work, the truncation happens at the one-loop level. While tree-level predictions are independent of any influences by higher-order cumulants, the one-loop correction to a cumulant of order n accounts for the tree-level contribution from the $(n + 1)$ -order cumulant. We justify this truncation for specific network models by comparing it to numerical simulations. A more general justification can be derived, if the loop contributions can be related to a small parameter like the inverse network size [62].

For parameter regimes where the truncation is meaningful, corrections to spike train cumulants can be calculated using the loop expansion. We found a way to make these predictions more robust by analytically solving the loop integrals.

As calculations are very extensive even for low-order cumulants, a systematic implementation using computer algebra is indispensable. This can be done, for example, as in theoretical particle physics using programs like FEYNARTS [63] and FORMCALC [64], which are written in `mathematica`[®]. All contributing graph topologies have to be generated first. The procedure used for the graph generation can be directly implemented, but a mathematically rigorous proof of completeness is still missing. This is essential in order not to forget any term of a given order in the series expansion, as it has happened previously for seemingly simple corrections of second-order cumulants [30]. Individual graphs are then translated into formulas by making use of the Feynman rules for the stochastic process under consideration. A

cascade of calculations is then performed on these expressions by making use of the new results explained above. Loop integrals can be replaced by sums over residuals, which can be calculated in a standardized way. Having such a machinery at hand allows to easily obtain more accurate predictions for stationary spiking statistics.

Based on the theoretical description of a stochastic process, the approach presented here makes quantitative and testable predictions for spike train statistics. Specifically, we were able to compute second-order cumulants for all individual tuples of neurons. As a result, full distributions of spike train cumulants, and not just their mean and variance, can be computed for given neuronal populations. Although the corrections due to an instantaneous nonlinearity are small, they can be nevertheless important. Spike-timing-dependent structural plasticity, for example, depends on the second-order cumulant of activity [65]. Small accumulating errors in theoretical predictions can cause large discrepancies of the predicted network structure. In homeostatic structural plasticity [66], in contrast, the degree of each node depends on its activity working point in a nonlinear manner. Small discrepancies in the working point prediction yields wrong degree predictions. Especially for non-normally distributed firing rates, like for example heavy-tailed log-normal distributions, it is important to know the entire distribution and not just its first two moments.

A final remark concerns the magnitude of individual diagram contributions. Although it is consistent to take all diagrams with a given number of loops into account, these do not automatically provide corrections of comparable magnitude. Depending on the parameters, specific diagrams can make much stronger contributions than others. The size of the contribution depends, for example, on the number of internal filter edges, or different occurrences of nonlinear gain function derivatives. Additionally, single diagrams may specifically correct cumulant predictions for certain subsets of neurons. A systematic investigation of these individual contributions would provide further insight into structure-dynamics relations. For future analyses of this type, it comes handy to have the explicit analytical dependencies of the loop integrals available. In total, these investigations greatly advance our understanding of how nonlinearities shape the cumulant distributions in networks.

Abbreviations

cdf, cumulative distribution function; LNP, linear-nonlinear Poisson; pdf, probability density functional; STDP, spike-timing dependent plasticity

Declarations

Ethics approval and consent to participate

Not applicable.

Consent for publication

Not applicable.

Availability of data and material

The simulation software scripts and generated data used and analysed during the current study are available from the corresponding author on reasonable request.

Competing interests

The authors declare that they have no competing interests.

Funding

The authors acknowledge support by the state of Baden-Württemberg through bwHPC and the German Research Foundation (DFG) through grant no INST 39/963-1 FUGG (bwForCluster NEMO). The research reported here has received additional funding from the European Union's Seventh Framework Programme (FP7/2007-2013) under Grant Agreement 600925 (NeuroSeeker), from BrainLinks-BrainTools, Cluster of Excellence funded by the German Research Foundation (DFG, grant number EXC 1086), and from the Carl Zeiss Stiftung.

Authors' contributions

The study was conceived and designed by MK and SR. Simulations, calculations and analysis of data was performed by MK. MK and SR drafted and revised the manuscript of the publication and approved its final version.

Acknowledgements

The authors are grateful to *Stojan Jovanović*, *Christopher Kim*, and *Nebojša Gašparović* for their advice and helpful discussions.

References

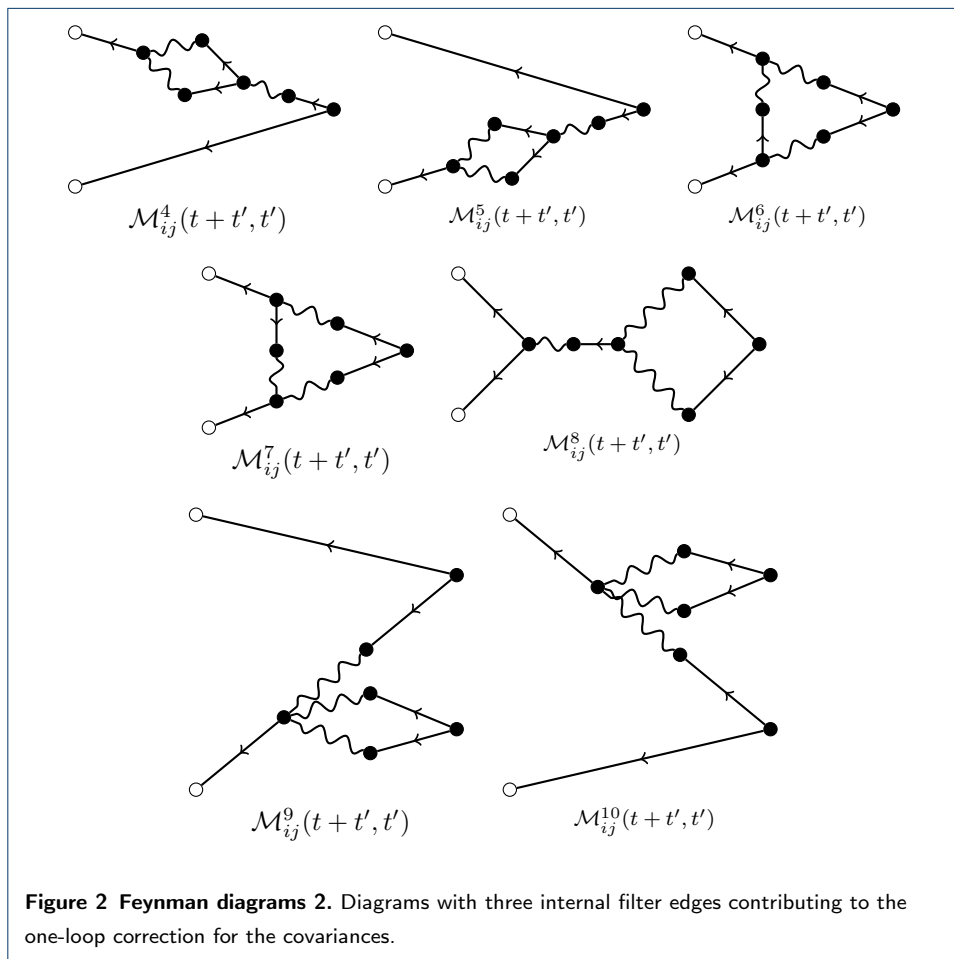
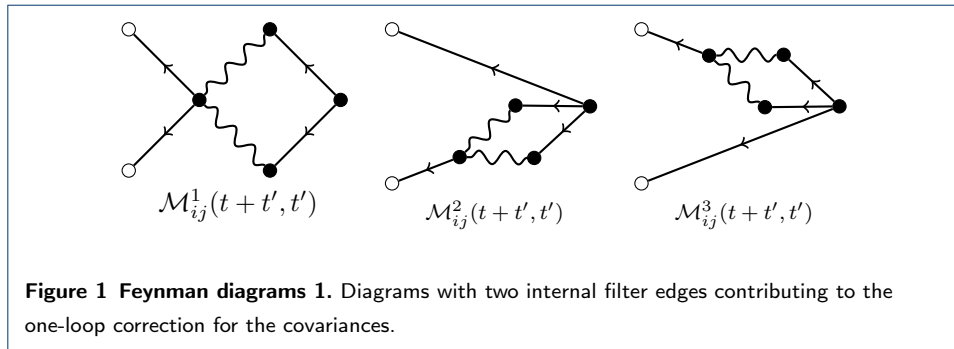
- Barthó, P., Hirase, H., Monconduit, L., Zugaro, M., Harris, K.D., Buzsáki, G.: Characterization of Neocortical Principal Cells and Interneurons by Network Interactions and Extracellular Features. *J Neurophysiol* **92**(1), 600–608 (2004). doi:[10.1152/jn.01170.2003](https://doi.org/10.1152/jn.01170.2003)
- Peyrache, A., Dehghani, N., Eskandar, E.N., Madsen, J.R., Anderson, W.S., Donoghue, J.A., Hochberg, L.R., Halgren, E., Cash, S.S., Destexhe, A.: Spatiotemporal dynamics of neocortical excitation and inhibition during human sleep. *Proceedings of the National Academy of Sciences* **109**(5), 1731–1736 (2012). doi:[10.1073/pnas.1109895109](https://doi.org/10.1073/pnas.1109895109)
- Lee, W.-C.A., Bonin, V., Reed, M., Graham, B.J., Hood, G., Glattfelder, K., Reid, R.C.: Anatomy and function of an excitatory network in the visual cortex. *Nature* **532**(7599), 370–374 (2016). doi:[10.1038/nature17192](https://doi.org/10.1038/nature17192)
- Kleinfeld, D., Bharioke, A., Blinder, P., Bock, D.D., Briggman, K.L., Chklovskii, D.B., Denk, W., Helmstaedter, M., Kaufhold, J.P., Lee, W.-C.A., Meyer, H.S., Micheva, K.D., Oberlaender, M., Prohaska, S., Reid, R.C., Smith, S.J., Takemura, S., Tsai, P.S., Sakmann, B.: Large-Scale Automated Histology in the Pursuit of Connectomes. *J Neurosci* **31**(45), 16125–16138 (2011). doi:[10.1523/JNEUROSCI.4077-11.2011](https://doi.org/10.1523/JNEUROSCI.4077-11.2011)

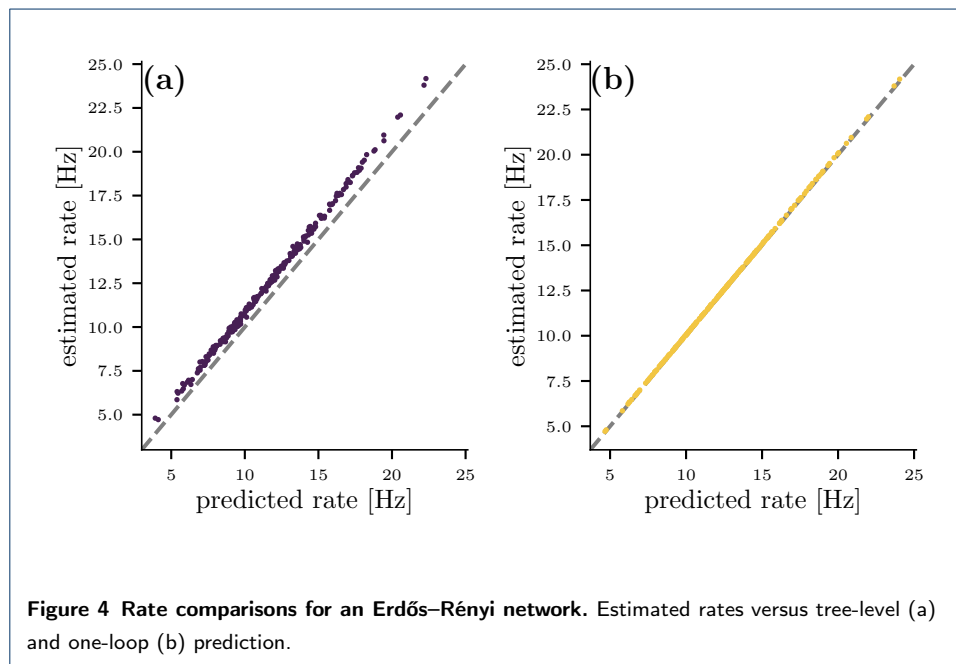
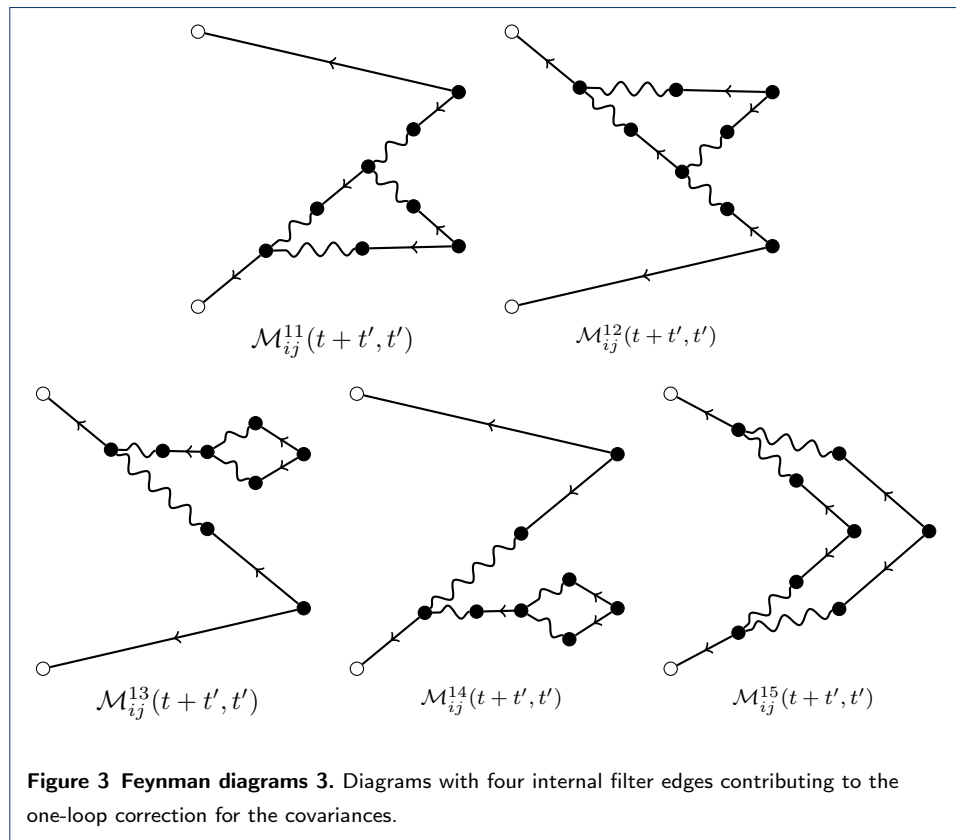
5. Takemura, S.-y., Bharioke, A., Lu, Z., Nern, A., Vitaladevuni, S., Rivlin, P.K., Katz, W.T., Olbris, D.J., Plaza, S.M., Winston, P., Zhao, T., Horne, J.A., Fetter, R.D., Takemura, S., Blazek, K., Chang, L.-A., Ogundeyi, O., Saunders, M.A., Shapiro, V., Sigmund, C., Rubin, G.M., Scheffer, L.K., Meinertzhagen, I.A., Chklovskii, D.B.: A visual motion detection circuit suggested by *Drosophila* connectomics. *Nature* **500**(7461), 175–181 (2013). doi:[10.1038/nature12450](https://doi.org/10.1038/nature12450)
6. Helmstaedter, M., Briggman, K.L., Turaga, S.C., Jain, V., Seung, H.S., Denk, W.: Connectomic reconstruction of the inner plexiform layer in the mouse retina. *Nature* **500**(7461), 168–174 (2013). doi:[10.1038/nature12346](https://doi.org/10.1038/nature12346)
7. Briggman, K.L., Helmstaedter, M., Denk, W.: Wiring specificity in the direction-selectivity circuit of the retina. *Nature* **471**(7337), 183–188 (2011). doi:[10.1038/nature09818](https://doi.org/10.1038/nature09818)
8. Bock, D.D., Lee, W.-C.A., Kerlin, A.M., Andermann, M.L., Hood, G., Wetzel, A.W., Yurgenson, S., Soucy, E.R., Kim, H.S., Reid, R.C.: Network anatomy and *in vivo* physiology of visual cortical neurons. *Nature* **471**(7337), 177–182 (2011). doi:[10.1038/nature09802](https://doi.org/10.1038/nature09802)
9. Kasthuri, N., Hayworth, K.J., Berger, D.R., Schalek, R.L., Conchello, J.A., Knowles-Barley, S., Lee, D., Vázquez-Reina, A., Kaynig, V., Jones, T.R., Roberts, M., Morgan, J.L., Tapia, J.C., Seung, H.S., Roncal, W.G., Vogelstein, J.T., Burns, R., Sussman, D.L., Priebe, C.E., Pfister, H., Lichtman, J.W.: Saturated Reconstruction of a Volume of Neocortex. *Cell* **162**(3), 648–661 (2015). doi:[10.1016/j.cell.2015.06.054](https://doi.org/10.1016/j.cell.2015.06.054)
10. Mishchenko, Y., Hu, T., Spacek, J., Mendenhall, J., Harris, K.M., Chklovskii, D.B.: Ultrastructural Analysis of Hippocampal Neuropil from the Connectomics Perspective. *Neuron* **67**(6), 1009–1020 (2010). doi:[10.1016/j.neuron.2010.08.014](https://doi.org/10.1016/j.neuron.2010.08.014)
11. Herz, A.V.M., Gollisch, T., Machens, C.K., Jaeger, D.: Modeling Single-Neuron Dynamics and Computations: A Balance of Detail and Abstraction. *Science* **314**(5796), 80–85 (2006). doi:[10.1126/science.1127240](https://doi.org/10.1126/science.1127240)
12. Koch, C., Segev, I.: Methods in Neuronal Modeling: From Ions to Networks, 2nd edn. Computational Neuroscience Series. The MIT Press, Cambridge, Massachusetts (2001)
13. Stein, R.B.: A Theoretical Analysis of Neuronal Variability. *Biophysical Journal* **5**(2), 173–194 (1965)
14. Brunel, N.: Dynamics of Sparsely Connected Networks of Excitatory and Inhibitory Spiking Neurons. *J Comput Neurosci* **8**(3), 183–208 (2000). doi:[10.1023/A:1008925309027](https://doi.org/10.1023/A:1008925309027)
15. Hawkes, A.G.: Spectra of Some Self-Exciting and Mutually Exciting Point Processes. *Biometrika* **58**(1), 83–90 (1971). doi:[10.2307/2334319](https://doi.org/10.2307/2334319)
16. Hawkes, A.G.: Point Spectra of Some Mutually Exciting Point Processes. *J R Stat Soc Ser B* **33**(3), 438–443 (1971). doi:[10.1111/j.2517-6161.1971.tb01530.x](https://doi.org/10.1111/j.2517-6161.1971.tb01530.x)
17. Pernice, V., Staude, B., Cardanobile, S., Rotter, S.: How Structure Determines Correlations in Neuronal Networks. *PLoS Comput Biol* **7**(5), 1002059 (2011). doi:[10.1371/journal.pcbi.1002059](https://doi.org/10.1371/journal.pcbi.1002059)
18. Pernice, V., Staude, B., Cardanobile, S., Rotter, S.: Recurrent interactions in spiking networks with arbitrary topology. *Phys Rev E* **85**(3), 031916 (2012). doi:[10.1103/PhysRevE.85.031916](https://doi.org/10.1103/PhysRevE.85.031916)
19. Jovanović, S., Hertz, J., Rotter, S.: Cumulants of Hawkes point processes. *Physical Review E* **91**(4), 042802 (2015). doi:[10.1103/PhysRevE.91.042802](https://doi.org/10.1103/PhysRevE.91.042802)
20. Jovanović, S., Rotter, S.: Interplay between Graph Topology and Correlations of Third Order in Spiking Neuronal Networks. *PLoS Comput Biol* **12**(6), 1–28 (2016). doi:[10.1371/journal.pcbi.1004963](https://doi.org/10.1371/journal.pcbi.1004963)
21. Ostojic, S., Brunel, N.: From Spiking Neuron Models to Linear-Nonlinear Models. *PLoS Comput Biol* **7**(1), 1001056 (2011). doi:[10.1371/journal.pcbi.1001056](https://doi.org/10.1371/journal.pcbi.1001056)
22. Truccolo, W.: From point process observations to collective neural dynamics: Nonlinear Hawkes process GLMs, low-dimensional dynamics and coarse graining. *J Physiol Paris* **110**(4, Part A), 336–347 (2016). doi:[10.1016/j.jphysparis.2017.02.004](https://doi.org/10.1016/j.jphysparis.2017.02.004)
23. Pillow, J.W., Shlens, J., Paninski, L., Sher, A., Litke, A.M., Chichilnisky, E.J., Simoncelli, E.P.: Spatio-temporal correlations and visual signalling in a complete neuronal population. *Nature* **454**(7207), 995–999 (2008). doi:[10.1038/nature07140](https://doi.org/10.1038/nature07140)
24. Gerhard, F., Deger, M., Truccolo, W.: On the stability and dynamics of stochastic spiking neuron models: Nonlinear Hawkes process and point process GLMs. *PLoS Comput Biol* **13**(2), 1–31 (2017). doi:[10.1371/journal.pcbi.1005390](https://doi.org/10.1371/journal.pcbi.1005390)

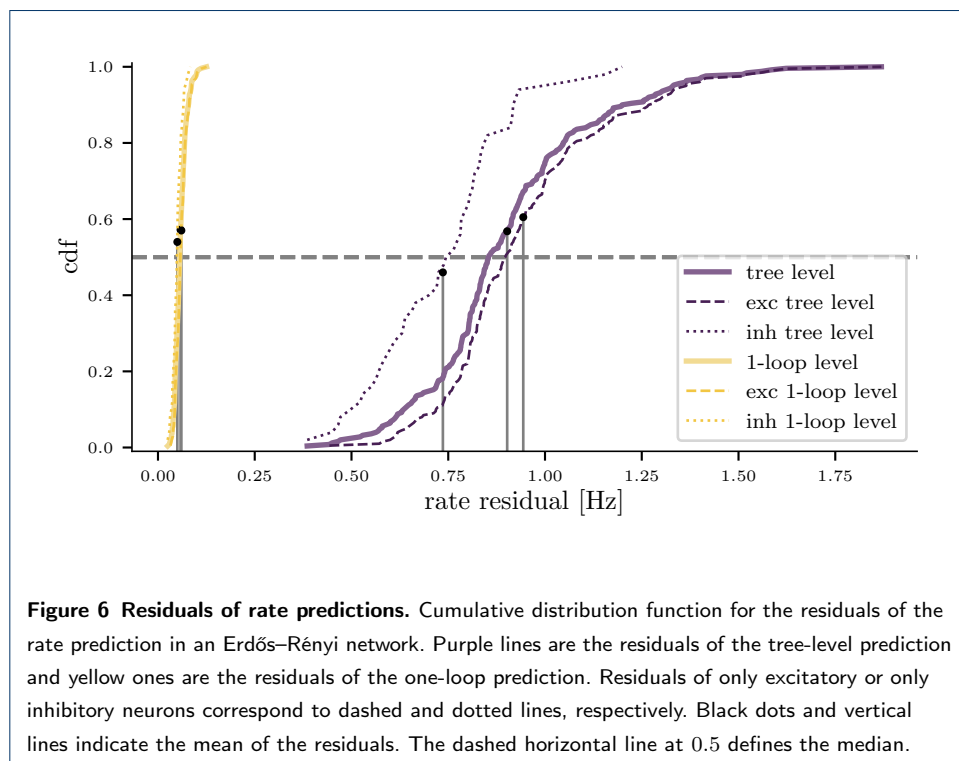
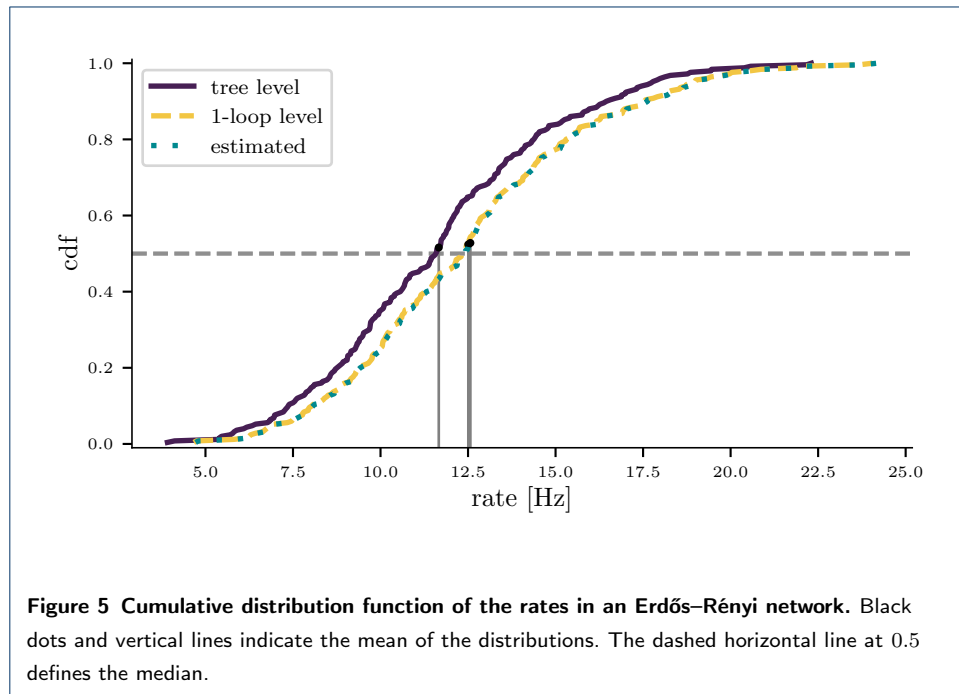
25. Lambert, R.C., Tuleau-Malot, C., Bessaih, T., Rivoirard, V., Bouret, Y., Leresche, N., Reynaud-Bouret, P.: Reconstructing the functional connectivity of multiple spike trains using Hawkes models. *J Neurosci Methods* (2017). doi:[10.1016/j.jneumeth.2017.12.026](https://doi.org/10.1016/j.jneumeth.2017.12.026)
26. Feldman, D.E.: The Spike-Timing Dependence of Plasticity. *Neuron* **75**(4), 556–571 (2012). doi:[10.1016/j.neuron.2012.08.001](https://doi.org/10.1016/j.neuron.2012.08.001)
27. Pfister, J.-P., Gerstner, W.: Triplets of Spikes in a Model of Spike Timing-Dependent Plasticity. *J Neurosci* **26**(38), 9673–9682 (2006). doi:[10.1523/JNEUROSCI.1425-06.2006](https://doi.org/10.1523/JNEUROSCI.1425-06.2006)
28. Shimazaki, H., Sadeghi, K., Ishikawa, T., Ikegaya, Y., Toyozumi, T.: Simultaneous silence organizes structured higher-order interactions in neural populations. *Sci Rep* **5**, 9821 (2015). doi:[10.1038/srep09821](https://doi.org/10.1038/srep09821)
29. Buice, M.A., Cowan, J.D., Chow, C.C.: Systematic Fluctuation Expansion for Neural Network Activity Equations. *Neural Comput* **22**(2), 377–426 (2010). doi:[10.1162/neco.2009.02-09-960](https://doi.org/10.1162/neco.2009.02-09-960)
30. Koch Ocker, G., Josić, K., Shea-Brown, E., Buice, M.A.: Linking structure and activity in nonlinear spiking networks. *PLoS Comput Biol* **13**(6), 1005583 (2017). doi:[10.1371/journal.pcbi.1005583](https://doi.org/10.1371/journal.pcbi.1005583)
31. Kass, R.E., Eden, U.T., Brown, E.N.: Analysis of Neural Data. Springer Series in Statistics. Springer New York, New York, NY (2014). doi:[10.1007/978-1-4614-9602-1](https://doi.org/10.1007/978-1-4614-9602-1)
32. Grün, S., Rotter, S.: Analysis of Parallel Spike Trains. Springer Series in Computational Neuroscience, vol. 7. Springer Boston, Boston, MA (2010). doi:[10.1007/978-1-4419-5675-0](https://doi.org/10.1007/978-1-4419-5675-0)
33. Cox, D.R., Isham, V.: Point Processes. Monographs on Statistics and Applied Probability, vol. 12. CRC Press, New York (1980)
34. Daley, D.J., Vere-Jones, D.: An Introduction to the Theory of Point Processes : Volume I: Elementary Theory and Methods. Probability and Its Applications. Springer, New York, NY, New York (2003)
35. Paninski, L.: Maximum likelihood estimation of cascade point-process neural encoding models. *Network* **15**(4), 243–262 (2004)
36. Simoncelli, E., Pillow, J.W., Paninski, L., Schwartz, O.: Characterization of neural responses with stochastic stimuli. In: Gazzaniga, M. (ed.) *The Cognitive Neurosciences*, 3rd edn., pp. 327–338. The MIT Press, Cambridge (2004)
37. Bremaud, P., Massoulié, L.: Stability of Nonlinear Hawkes Processes. *Ann Probab* **24**(3), 1563–1588 (1996). doi:[10.1214/aop/1065725193](https://doi.org/10.1214/aop/1065725193)
38. Delattre, S., Fournier, N., Hoffmann, M.: Hawkes processes on large networks. *Ann Appl Probab* **26**(1), 216–261 (2016). doi:[10.1214/14-AAP1089](https://doi.org/10.1214/14-AAP1089)
39. Truccolo, W., Eden, U.T., Fellows, M.R., Donoghue, J.P., Brown, E.N.: A Point Process Framework for Relating Neural Spiking Activity to Spiking History, Neural Ensemble, and Extrinsic Covariate Effects. *J Neurophysiol* **93**(2), 1074–1089 (2005). doi:[10.1152/jn.00697.2004](https://doi.org/10.1152/jn.00697.2004)
40. Nelder, J.A., Wedderburn, R.W.M.: Generalized Linear Models. *J R Stat Soc Ser A* **135**(3), 370–384 (1972). doi:[10.2307/2344614](https://doi.org/10.2307/2344614)
41. Cardanobile, S., Rotter, S.: Multiplicatively interacting point processes and applications to neural modeling. *J Comput Neurosci* **28**(2), 267–284 (2010). doi:[10.1007/s10827-009-0204-0](https://doi.org/10.1007/s10827-009-0204-0)
42. Weber, A.I., Pillow, J.W.: Capturing the Dynamical Repertoire of Single Neurons with Generalized Linear Models. *Neural Comput* **29**(12), 3260–3289 (2017). doi:[10.1162/neco_a_01021](https://doi.org/10.1162/neco_a_01021)
43. Amari, S.-I.: Homogeneous nets of neuron-like elements. *Biol Cybern* **17**(4), 211–220 (1975). doi:[10.1007/BF00339367](https://doi.org/10.1007/BF00339367)
44. Amari, S.-I.: Dynamics of pattern formation in lateral-inhibition type neural fields. *Biol Cybern* **27**(2), 77–87 (1977). doi:[10.1007/BF00337259](https://doi.org/10.1007/BF00337259)
45. Bressloff, P.C.: Path-Integral Methods for Analyzing the Effects of Fluctuations in Stochastic Hybrid Neural Networks. *J Math Neurosci* **5**(1), 1–33 (2015). doi:[10.1186/s13408-014-0016-z](https://doi.org/10.1186/s13408-014-0016-z)
46. Voronenko, S.O.: Nonlinear signal processing by noisy spiking neurons. PhD Thesis, Humboldt-Universität zu Berlin, Mathematisch-Naturwissenschaftliche Fakultät (2018). doi:[10.18452/18793](https://doi.org/10.18452/18793)
47. Campbell, P.: Dynamical implications of network statistics. PhD thesis, University of Minnesota (August 2014)
48. Doi, M.: Second quantization representation for classical many-particle system. *J Phys A Math Gen* **9**(9), 1465 (1976). doi:[10.1088/0305-4470/9/9/008](https://doi.org/10.1088/0305-4470/9/9/008)

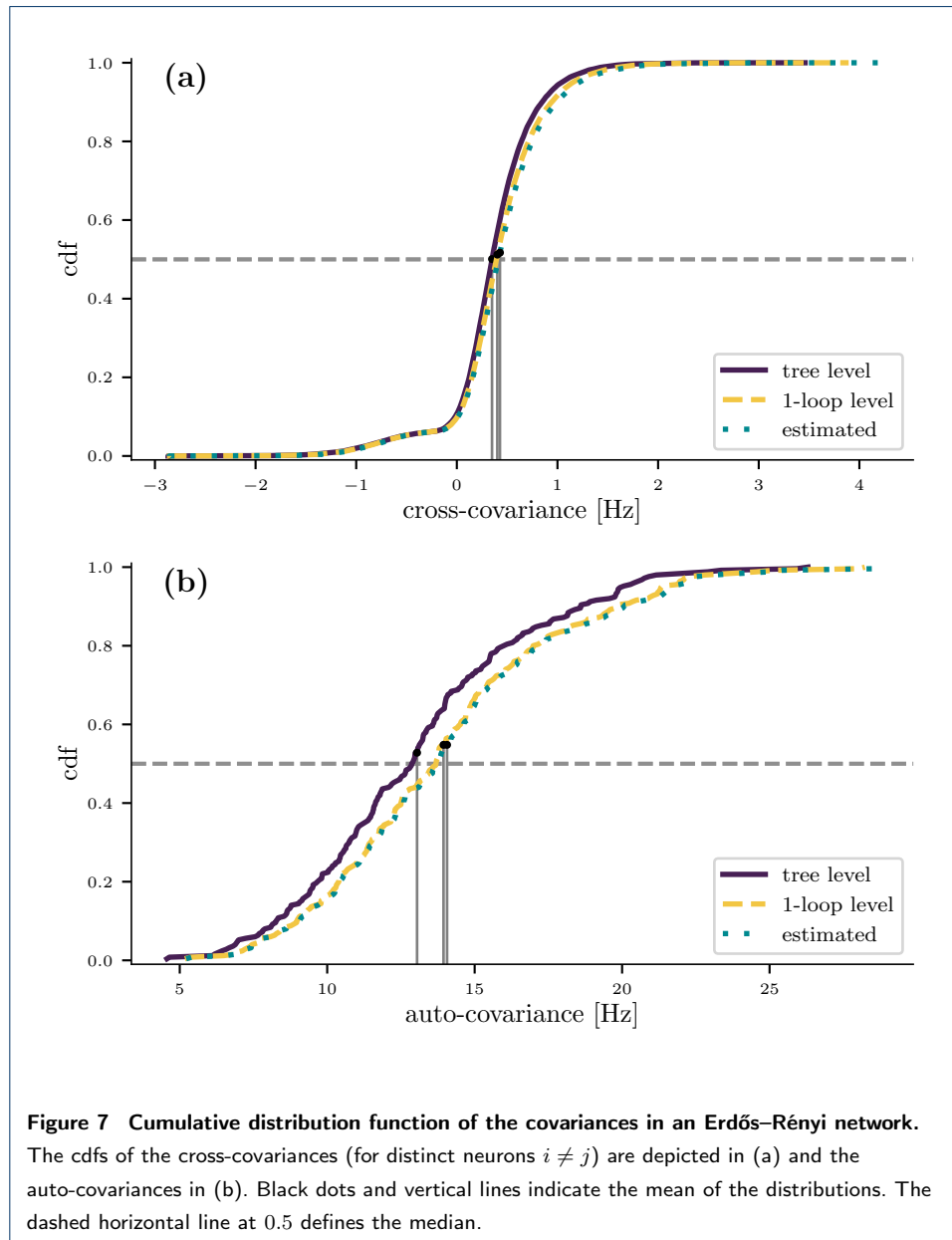
49. Doi, M.: Stochastic theory of diffusion-controlled reaction. *J Phys A Math Gen* **9**(9), 1479 (1976). doi:[10.1088/0305-4470/9/9/009](https://doi.org/10.1088/0305-4470/9/9/009)
50. Peliti, L.: Path integral approach to birth-death processes on a lattice. *Journal de Physique* **46**(9), 1469–1483 (1985). doi:[10.1051/jphys:019850046090146900](https://doi.org/10.1051/jphys:019850046090146900)
51. Martin, P.C., Siggia, E.D., Rose, H.A.: Statistical Dynamics of Classical Systems. *Phys Rev A* **8**(1), 423–437 (1973). doi:[10.1103/PhysRevA.8.423](https://doi.org/10.1103/PhysRevA.8.423)
52. Täuber, U.C.: Field-Theory Approaches to Nonequilibrium Dynamics. In: Henkel, M., Pleimling, M., Sanctuary, R. (eds.) *Ageing and the Glass Transition. Lecture Notes in Physics*, pp. 295–348. Springer Berlin Heidelberg, Berlin, Heidelberg (2007). doi:[10.1007/3-540-69684-9_7](https://doi.org/10.1007/3-540-69684-9_7)
53. Lefèvre, A., Biroli, G.: Dynamics of interacting particle systems: Stochastic process and field theory. *J Stat Mech* **2007**(07), 07024 (2007). doi:[10.1088/1742-5468/2007/07/P07024](https://doi.org/10.1088/1742-5468/2007/07/P07024)
54. Buice, M.A., Cowan, J.D.: Field-theoretic approach to fluctuation effects in neural networks. *Phys Rev E* **75**(5), 051919 (2007). doi:[10.1103/PhysRevE.75.051919](https://doi.org/10.1103/PhysRevE.75.051919)
55. Chow, C.C., Buice, M.A.: Path Integral Methods for Stochastic Differential Equations. *J Math Neurosci* **5**, 8 (2015). doi:[10.1186/s13408-015-0018-5](https://doi.org/10.1186/s13408-015-0018-5)
56. Stapmanns, J., Kühn, T., Dahmen, D., Luu, T., Honerkamp, C., Helias, M.: Self-consistent formulations for stochastic nonlinear neuronal dynamics. *arXiv preprint* (2018). [1812.09345](https://arxiv.org/abs/1812.09345)
57. Lang, S.: *Complex Analysis*. Springer New York, New York, NY (1999). doi:[10.1007/978-1-4757-3083-8](https://doi.org/10.1007/978-1-4757-3083-8)
58. Bernard, C., Ge, Y.C., Stockley, E., Willis, J.B., Wheal, H.V.: Synaptic integration of NMDA and non-NMDA receptors in large neuronal network models solved by means of differential equations. *Biol Cybern* **70**(3), 267–273 (1994). doi:[10.1007/BF00197607](https://doi.org/10.1007/BF00197607)
59. Tuckwell, H.C.: *Introduction to Theoretical Neurobiology: Volume 1, Linear Cable Theory And Dendritic Structure*. Cambridge Studies in Mathematical Biology. Cambridge University Press, Cambridge (1988). doi:[10.1017/CBO9780511623271](https://doi.org/10.1017/CBO9780511623271)
60. Rotter, S., Diesmann, M.: Exact digital simulation of time-invariant linear systems with applications to neuronal modeling. *Biol Cybern* **81**, 381–402 (1999). doi:[10.1007/s004220050570](https://doi.org/10.1007/s004220050570)
61. Jones, E., Oliphant, T., Peterson, P., et al.: *SciPy: Open source scientific tools for Python* (2001). [Online, www.scipy.org; accessed 2020-01-11]
62. Bressloff, P.: Stochastic Neural Field Theory and the System-Size Expansion. *SIAM J Appl Math* **70**(5), 1488–1521 (2009). doi:[10.1137/090756971](https://doi.org/10.1137/090756971)
63. Hahn, T.: Generating Feynman diagrams and amplitudes with FeynArts 3. *Comput Phys Commun* **140**(3), 418–431 (2001). doi:[10.1016/S0010-4655\(01\)00290-9](https://doi.org/10.1016/S0010-4655(01)00290-9)
64. Hahn, T., Pérez-Victoria, M.: Automated one-loop calculations in four and D dimensions. *Comput Phys Commun* **118**(2), 153–165 (1999). doi:[10.1016/S0010-4655\(98\)00173-8](https://doi.org/10.1016/S0010-4655(98)00173-8)
65. Deger, M., Helias, M., Rotter, S., Diesmann, M.: Spike-Timing Dependence of Structural Plasticity Explains Cooperative Synapse Formation in the Neocortex. *PLoS Comput Biol* **8**(9), 1002689 (2012). doi:[10.1371/journal.pcbi.1002689](https://doi.org/10.1371/journal.pcbi.1002689)
66. Gallinaro, J.V., Rotter, S.: Associative properties of structural plasticity based on firing rate homeostasis in recurrent neuronal networks. *Scientific Reports* **8**(1), 3754 (2018). doi:[10.1038/s41598-018-22077-3](https://doi.org/10.1038/s41598-018-22077-3)

Figures









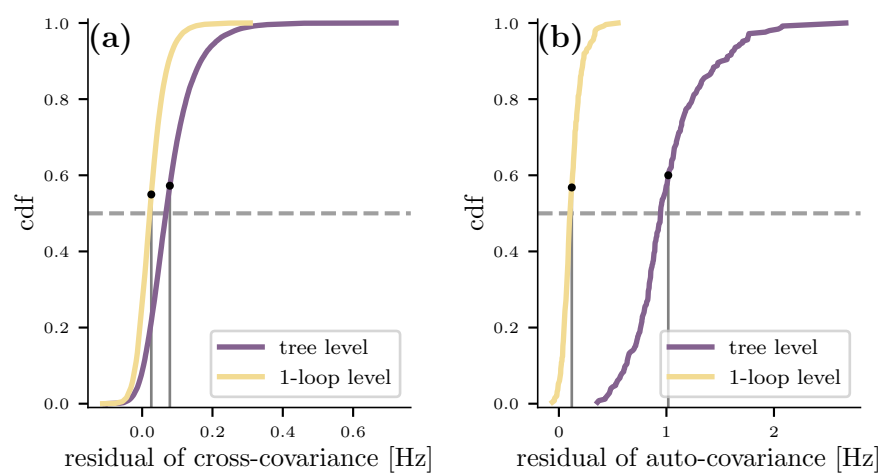


Figure 8 Residuals of covariance predictions. The cdfs are shown separately for cross- and auto-covariances in (a) and (b), respectively. Black dots and vertical lines indicate the mean of the residuals. The dashed horizontal line at 0.5 defines the median.